nature neuroscience

ARTICLES

https://doi.org/10.1038/s41593-018-0239-5

Triple dissociation of attention and decision computations across prefrontal cortex

Laurence T. Hunt[1,2,3,4,7*], W. M. Nishantha Malalasekera[1,7], Archy O. de Berker[1,2], Bruno Miranda[1,5,6], Simon F. Farmer[1], Timothy E. J. Behrens[2,3] and Steven W. Kennerley[1*]

Naturalistic decision-making typically involves sequential deployment of attention to choice alternatives to gather information before a decision is made. Attention filters how information enters decision circuits, thus implying that attentional control may shape how decision computations unfold. We recorded neuronal activity from three subregions of the prefrontal cortex (PFC) while monkeys performed an attention-guided decision-making task. From the first saccade to decision-relevant information, a triple dissociation of decision- and attention-related computations emerged in parallel across PFC subregions. During subsequent saccades, orbitofrontal cortex activity reflected the value comparison between currently and previously attended information. In contrast, the anterior cingulate cortex carried several signals reflecting belief updating in light of newly attended information, the integration of evidence to a decision bound and an emerging plan for what action to choose. Our findings show how anatomically dissociable PFC representations evolve during attention-guided information search, supporting computations critical for value-guided choice.

Anatomical[1,2], neuroimaging[3,4] and lesion studies[5,6] have indicated that the PFC is central to value-guided choice. These techniques have functionally localized subcomponents of decision-making to different subregions of the PFC. However, explanations of neuronal computations within these subregions vary widely across studies. Recent debates on the roles of PFC subregions in value-guided decision-making have been manifold. One debate centers on whether decision-related computations are performed in series (with certain subregions preceding others) or in parallel (with activity simultaneously distributed across subregions)[7,8]. A second debate concerns whether stimulus valuation in the orbitofrontal cortex (OFC) and adjacent ventromedial prefrontal cortex may be influenced by attention[9–11]. Further debate relates to whether the anterior cingulate cortex (ACC) integrates evidence for different actions[12–15], modifies behavior in light of new evidence[16–19] or evaluates evidence for alternative courses of action[20,21]. Resolving these debates demands a rich dataset that contrasts neuronal activity across multiple PFC subregions within a single paradigm, while the order, duration and frequency with which choice options are attended to and compared are experimentally controlled.

Real-world choices are typically guided by multiple shifts in attention among choice alternatives. Interactions among attention, information search and choice have been widely studied in the behavioral sciences[22–28], and the order, duration and frequency of shifts in visual attention can strongly influence the eventual decision made[24]. The evolutionary expansion of the PFC in primates relative to other species may have been driven by primates' need to foveate, evaluate, remember and compare alternatives during visually guided foraging[29]. However, how attentional reorienting affects PFC computations performed at a neuronal level during choice remains largely unknown[30]. This lack of knowledge is because decision paradigms in neuroscience have been predominantly conducted with central or uncontrolled fixation; consequently, attentional focus is not placed under experimental control. By determining which information enters decision circuits, attention affects the temporal dynamics of several decision-related computations, including stimulus identification, valuation, comparison to previously attended alternatives and action selection. Dissociating the neural substrates of decision-related computations across the PFC may therefore require synchronizing neural activity with attentional focus.

Here, we contrasted neuronal activity in the macaque OFC, ACC and dorsolateral prefrontal cortex (DLPFC) during sequential attention-guided information search and choice. We found that when attention is first deployed to a choice alternative, a triple dissociation of attention and decision computations emerges in parallel across these three areas. As further information is sampled, the OFC carries representations required for comparing currently and previously attended information. In contrast, multiple signals in the ACC reflect belief updating in light of new evidence and relative valuation of different actions. These signals ramp toward final commitment to a choice. Our findings are consistent with models describing value comparison as an attention-guided bounded diffusion process[24] as well as with more recent accounts that frame economic choice as a series of accept/reject decisions[31].

Results

Experimental paradigm and subject behavior. Our task design (Fig. 1a) mirrored that in established behavioral studies examining attention-guided information search during sequential, multiattribute choice[22,25,26,32]. Each option, presented on the left and right sides of the screen, comprised two prelearned picture cues representing different attributes: the probability and magnitude of a juice reward. Crucially, at the start of the trial, all cues were hidden. Behavioral and neuronal data were collected from two macaque monkeys

[1]Sobell Department of Motor Neuroscience, University College London, London, UK. [2]Wellcome Centre for Human Neuroimaging, University College London, London, UK. [3]Wellcome Centre for Integrative Neuroimaging, University of Oxford, Oxford, UK. [4]Oxford Health NHS Foundation Trust, Oxford, UK. [5]International Neuroscience Doctoral Programme, Champalimaud Foundation, Lisbon, Portugal. [6]Instituto de Medicina Molecular, Faculdade de Medicina, Universidade de Lisboa, Lisbon, Portugal. [7]These authors contributed equally: Laurence T. Hunt, W. M. Nishantha Malalasekera. *e-mail: laurence.hunt@psych.ox.ac.uk; s.kennerley@ucl.ac.uk

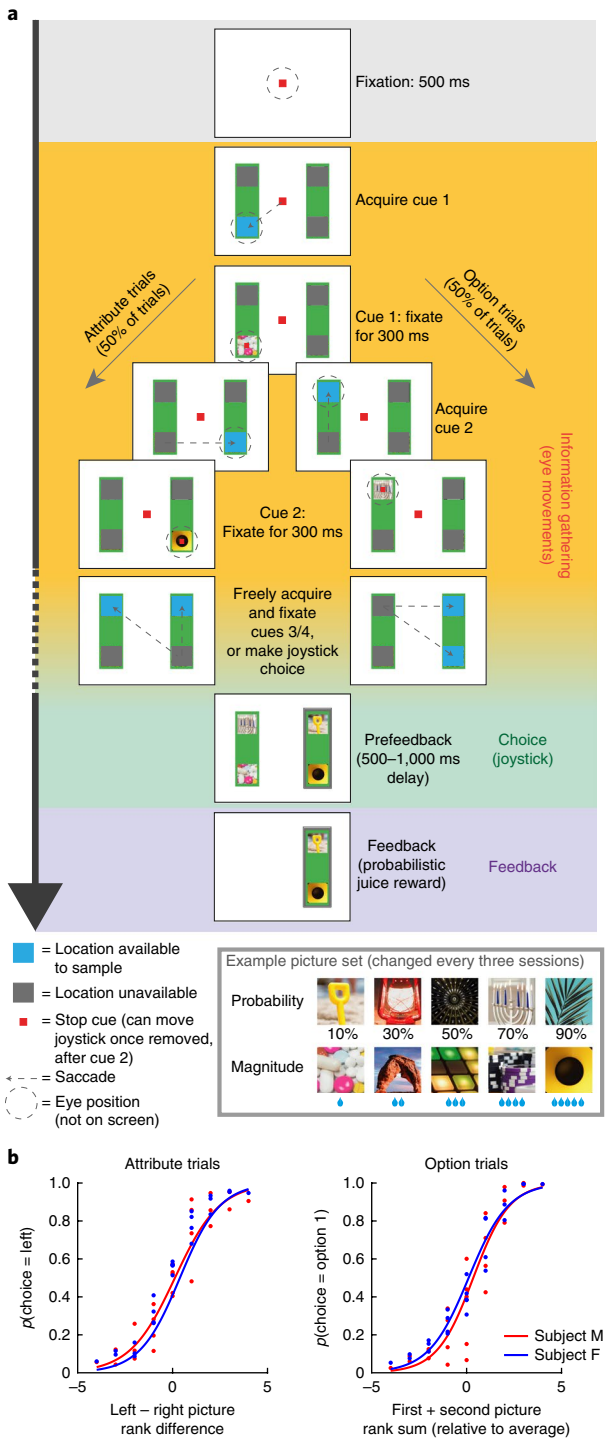

Fig. 1 | Experimental paradigm and basic subject behavior. a, Task design. Subjects chose between a left and right option (green rectangles) by using a manual joystick movement, after sequentially sampling two, three, or four cues that revealed reward probability and magnitude to the subject. Blue squares indicate locations available for information sampling. In attribute trials (left), cues 1 and 2 were on opposing options but the same attribute; in option trials (right), cues 1 and 2 were different attributes of the same option. **b**, Choice behavior as a function of cue 1 and cue 2 values. Left, probability of choosing the left option in attribute trials, as a function of the left – right picture rank difference (where 1 is the lowest-ranked picture in each attribute, and 5 is highest-ranked picture). Right, probability of choosing option 1 in option trials, as a function of the first-picture value plus the second-picture value (relative to the middle-value picture 3). Additional analyses of choices in Supplementary Fig. 1.

(*Macaca mulatta*). The subjects made an instructed saccade toward a highlighted location to reveal cue 1. After 300 ms of uninterrupted fixation, cue 1 was covered, and another location was highlighted, either vertically on the same option or horizontally on the same attribute. Subjects saccaded here to reveal cue 2, again for 300 ms. Hereafter, subjects could select either option by using a manual left/right joystick movement. Alternatively, they could fixate on one or both remaining highlighted cues in any order to reveal further information before making their decision. After the joystick choice, all four cues were revealed, and a juice reward was delivered with the chosen probability and magnitude. The picture cues, first/second highlighted locations and probability/magnitude attributes on the top versus bottom were pseudorandomly selected in each trial (with uniform distribution).

Both monkeys used cue values appropriately to guide their choices (Fig. 1b). They chose the option with higher expected value in 76.6% and 79.8% of trials (for subject F ($n = 25$ sessions) and subject M ($n = 32$ sessions), respectively), assigning approximately equal weight to reward probability and magnitude, and using all viewed cues to guide their choice (Supplementary Fig. 1a,b). However, most choices were based on partial information: the subjects chose before all four cues had been evaluated in 85.5% and 71.4% of trials (for F and M, respectively). The choice accuracy based on the pictures observed, rather than the true expected values, was substantially higher (86.3% and 87.4% for F and M, respectively). Unexpectedly, the choice accuracy was also higher in trials in which subjects sampled fewer pieces of information (Supplementary Fig. 1c). This result was because such trials were associated with a higher value difference, and subjects consequently terminated those trials more quickly (Supplementary Fig. 1d).

The subjects preferred to sample information from the option that they currently intended to choose[25,26]. This behavior revealed itself in two ways. First, subjects were free to choose where to attend with their third saccade. In 'attribute' trials, this saccade was preferentially directed toward the option with the higher relative expected value between cue 1 and cue 2 (Fig. 2a, comparison of bottom left versus top right). Such behavior mirrors a recently identified bias toward 'sampling the favorite' in an equivalent experiment in human participants[25] and mirrors classic 'confirmation biases' in human hypothesis testing[33]. Second, after two cues had been presented, the subjects were also free to decide when to stop sampling information and to commit to a final choice. In 'option' trials, subjects sampled the fewest pieces of information when cues 1 and 2 were highest in value but sampled the most information when cues 1 and 2 were lowest in value (Fig. 2b, comparison of bottom right versus top left). This result mirrors a (milder) 'positive evidence approach' bias in humans[25].

The latter bias (Fig. 2b) appears particularly surprising. Two low-valued cues in an option trial provide conclusive evidence for choosing the option not yet attended to. Yet the monkeys nonetheless sampled from that option before committing to choosing it. This behavior is suboptimal in the context of a two-alternative forced choice yet more rational in the context of real-world decisions that comprise multiple, non-mutually-exclusive alternatives. Here, evidence against one option does not provide evidence in favor of any particular alternative. A natural strategy for solving such choices is to consider one option to be the leading or 'foreground' candidate, and to decide whether to accept or reject it[31]. This accept/reject decision might still rely on value comparison, for example to the next best alternative[23,34] or the average reward rate of the environment[35].

Triply dissociable PFC population codes at the first saccade. We recorded single-unit activity from the ACC, DLPFC and OFC ($n = 189$, 135 and 183 neurons respectively; Fig. 3). ACC recordings were primarily from the dorsal bank of the cingulate sulcus (area 24);

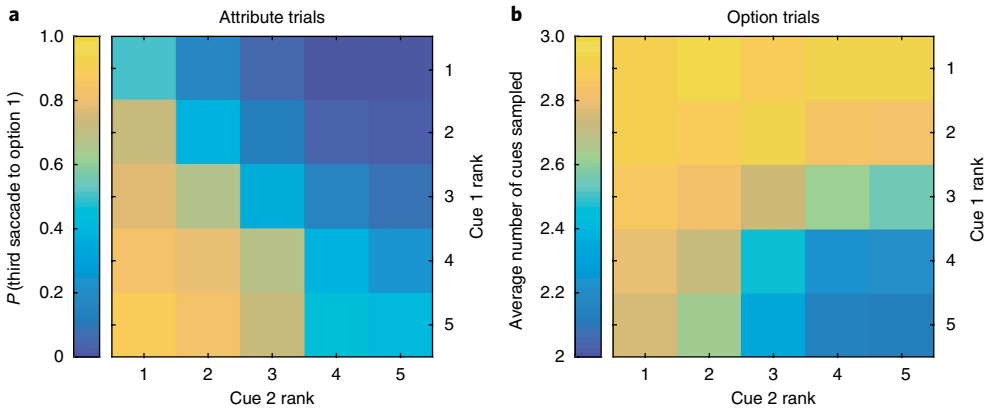

Fig. 2 | Information-sampling behavior in attribute and option trials reveals preference for sampling the current best alternative. a, In attribute trials in which a third cue was sampled, the probability of the third saccade being directed diagonally back toward option 1, rather than vertically to remain on option 2, is high when cue 1 has high value and cue 2 has low value. **b**, In option trials, the number of cues sampled is lowest when cues 1 and 2 have high value, but is highest when cues 1 and 2 have low value, even though complete information is provided about which option to choose.

OFC recordings were primarily from the medial orbital gyrus (area 13); and DLPFC recordings were primarily from the dorsal and ventral banks of the sulcus principalis (area 9/46).

A critical feature of our experiment is that after each saccade, the currently attended cue can be decomposed into multiple features: its associated attribute (magnitude or probability), value (level of reward probability or magnitude), spatial position (presentation on the top/bottom of screen), and action (left/right joystick response required to choose that option). In line with results from previous studies[36], we found a degree of PFC subregion specificity in single neurons encoding of these features (described below). However, there was substantial between-neuron heterogeneity in the decision-related computations encoded. This heterogeneity proved critical in robustly dissociating the computations performed by each subregion.

We capitalized on neuronal heterogeneity by assessing the population-level encoding of decision computations. At the time when cue 1 was attended to, we used representational similarity analysis (RSA). RSA correlates the normalized firing rate of the neural population among all conditions of interest[37]. This procedure characterizes task encoding across the neural population without strong prior assumptions regarding its structure. At cue 1 presentation, we performed RSA among 20 conditions: five probability cues and five magnitude cues, presented on either the left or the right option. Here, because neurons were not all simultaneously recorded, we performed the analysis on 'pseudopopulations'. For each subregion, we collapsed data across recording sessions and calculated the correlation matrix from the resulting [neurons × conditions] matrix of firing rates.

RSA revealed a striking triple dissociation of task-evoked neural codes across PFC subregions (Fig. 4a–c). This result was consistent across subjects (Supplementary Fig. 2). To formally compare the subregion specificity and temporal evolution of population representations, we regressed templates onto RSA matrices to capture different features of the task design. The DLPFC RSA reflected whether the subject was attending to the left or the right (Fig. 4d). The OFC representational similarity reflected the currently attended stimulus identity, irrespective of spatial position (Fig. 4e), and was also high for cues of similar attended value (Fig. 4f). The ACC and DLPFC RSAs showed a value code modulated by whether the subject was currently attending to the left or right option (Fig. 4g). The ACC RSA also divided high-valued and low-valued items such that variance in the ACC was best explained as a nonlinear, categorical function of value (Fig. 4h; labeled 'accept/reject' coding for reasons explored below).

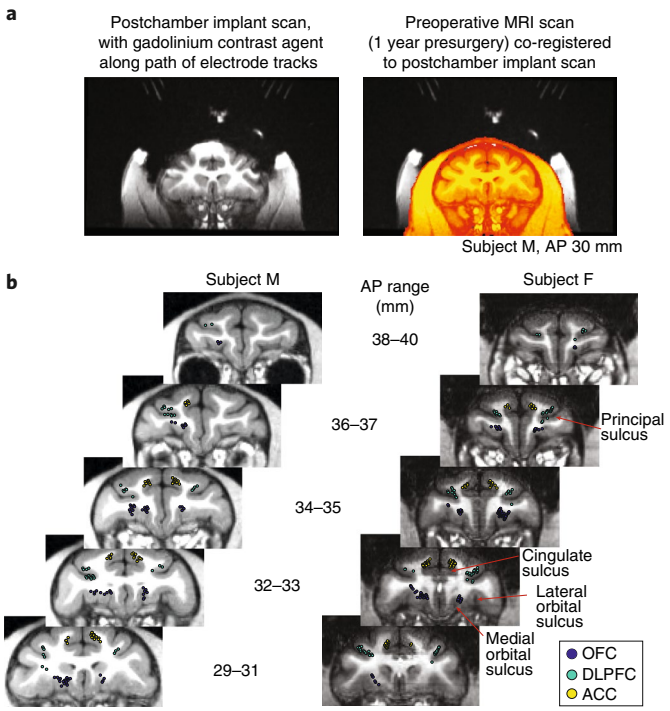

Fig. 3 | Recording locations. a, Strategy for reconstructing the paths of electrode tracks. Left, after surgery for chamber implantation, before craniotomy, the subjects underwent a magnetic resonance imaging (MRI) scan with a custom-built implant placed within the chamber. The MRI contrast agent gadolinium was contained along the trajectory of potential recording paths at regular 4-mm intervals. A prominent susceptibility artifact due to titanium chambers was present but did not affect the gadolinium trajectories, which were intentionally located away from the chamber. Right, this scan could be co-registered to a preoperative scan without susceptibility artifacts (in orange; notably, the head appears smaller, owing to muscle growth between scans), to reliably reconstruct recording locations. This technique was further verified by identification of gray/white-matter boundaries during the lowering of electrodes along different trajectories. **b**, Recording locations of OFC, DLPFC and ACC neurons, shown in coronal sections. Anterior–posterior (AP) range denotes the position anterior to the interaural plane in stereotactic coordinates.

For intuition, we have provided single-neuron examples for these features in Supplementary Fig. 3. We also present RSA matrices subdivided by top/bottom spatial position in Supplementary Fig. 4. It is important to acknowledge that there is not 'pure selectivity' for any one feature in a given region; for example, spatial attention is represented in both the OFC and ACC (Fig. 4d), and other task features have some degree of representation in multiple regions. Nonetheless, there is strong regional specificity in the degree to which different subregions encode each feature.

Decision-related computations at cue 1 emerged in parallel across the PFC rather than sequentially (Fig. 4d–h). We observed the temporal order and evolution of these different computations (Supplementary Video 1), and we also plotted the time courses of the coefficient of partial determination (CPD) sorted by region (Supplementary Fig. 5). We quantified the time at which information relating to different factors was encoded in different subregions by analyzing when the CPD in Fig. 4d–h reached 75% of its maximum value (t_{75}; Supplementary Fig. 5b,c). Spatial attention affected representational similarity around the time of the saccadic eye movement (t_{75} = 24 ms in the ACC, 72 ms in the DLPFC and 67 ms in the OFC). The early rise in the time of this effect can be attributed to saccade generation, because cue onset was time-locked to the saccade. Subsequently, the coding of stimulus identity and attended value (t_{75} = 269 ms/241 ms, respectively, in the OFC) were comparable in latency to accept/reject coding (t_{75} = 238 ms in the ACC and 224 ms in the OFC). In contrast, action value coding emerged significantly later (t_{75} = 457 ms in the ACC and 369 ms in the DLPFC). In summary, attentional modulation occurred at the time of the saccade; stimulus identification, valuation and accept/reject coding emerged in parallel across the OFC and ACC; the final representation to emerge was of action value.

Value encoding also differed between the ACC and OFC. The RSA in the OFC was consistent with a linear representation of cue 1 attended value (Fig. 4a,f). Additional analyses confirmed this result's robustness to the exact formulation of the 'attended value' template (Supplementary Note and Supplementary Figs. 11 and 12). We hypothesized that this graded signal in the OFC might be a substrate critical to support comparison of the currently attended cue value versus previously attended (stored) cue values during subsequent saccades[9,10,38].

In contrast, the ACC value coding was more nonlinear and categorical (Fig. 4h). Guided by the recent literature on ACC encoding expectancy violations and adapting behavior in light of new evidence[14,16–18,20,21,34], as well as the pattern of information sampling in Fig. 2, we hypothesized that ACC activity might reflect the decision of whether to accept or reject the current foreground option. In particular, a high-valued cue 1 might confirm the belief that the first attended option should be accepted, not rejected. This option would remain the foreground candidate, from which subjects would probably sample further information[25,31,33] (Fig. 2). In contrast, low-valued cues would disconfirm this belief, thus leading to the item being rejected and the alternative becoming the foreground option. This hypothesis can be more robustly evaluated during subsequent saccades, because subsequent cues might confirm or disconfirm the current foreground candidate as the best choice[34]. This signal might become particularly prominent before choice, when confirmatory evidence becomes sufficient to commit to an action.

Attention-guided value comparison in the OFC. To address our hypothesis concerning attention-guided value comparison in the OFC, we used multiple linear regression to evaluate how strongly each neuron encoded the values of cues 1, 2, 3 and 4 across time in both option and attribute trials. We plotted the average CPD (a measure of variance explained by each regressor; Methods), which was time-locked to each of the first three cues (Fig. 5a). The results showed that value encoding by OFC neurons peaked approximately 300 ms after each cue was revealed but was then sustained above baseline as further cues were attended. Notably, the CPD values in these single-neuron analyses were considerably lower than those in Fig. 4f but comparable to those in other studies of value-based decision-making[39,40]. This result was because these values reflect variance explained across trials in each neuron, whereas the values in Fig. 4f reflect variance explained across the neural population (having averaged across trials for each condition).

Crucially, neuronal encoding of value was highly variable across the population. We again capitalized on this heterogeneity to define population task-related 'subspaces' for value encoding. Task-related subspaces can be defined by using linear regression to determine how sensitive each neuron is to experimental variables of interest, and then projecting the data into a space defined by these regression coefficients[41]. This analysis can again be performed on pseudopopulations of nonsimultaneously recorded neurons, because the regression is performed separately (within a session) for each neuron, before the collapsing of data across sessions to define the (pseudo)population subspace.

For example, we found that the single-neuron t statistics for the regression of the cue 1 value when cue 1 was attended to (ordinate in Fig. 5b) correlated positively with the t statistics for the cue 2 value when cue 2 was attended to (abscissa in Fig. 5b). These two regressors are orthogonal and defined at different task epochs (by using a window of 150–350 ms after stimulus onset for each cue). This analysis therefore reveals a stable population subspace for the currently attended cue value.

We repeated this approach for different phases of the task, to determine how the currently attended cue value subspace (ordinates in Fig. 5c–e) correlated with subspaces encoding previously attended, or stored, cues across time (abscissae in Fig. 5c–e). The results revealed a signature of value comparison in the OFC between currently and previously attended cues[10]. For example, when cue 2 was attended to in attribute trials, the currently attended cue 2 value subspace correlated negatively with the stored cue 1 value subspace, representing the other option (Fig. 5c). This negative correlation indicated that neurons encoding the value of the currently attended option at cue do so relative to the value of the previously attended option, a key prediction of recent models of economic choice[24,31]. Similarly, when cue 3 was attended to in option trials, the stored cue 1 and stored cue 2 values both represented the other option and were both negatively correlated with the currently attended cue 3 value subspace (Fig. 5d,e). However, these two stored subspaces were themselves positively correlated at cue 3 in option trials (Fig. 5f). These results demonstrate that the two previously attended cues were combined at cue 3 to allow for comparison with the currently attended cue.

A more comprehensive description of the interaction between attention and value was obtained by plotting the cross-correlation of these subspaces across time (Fig. 5g–j). This plot revealed how the same OFC population subspace dynamically shifts its encoding of values from positive to negative as the subject saccades around the screen. The letters superimposed on these plots refer to the correlations shown in Fig. 5b–f.

Importantly, this signature of attention-guided value comparison was unique to the OFC. Whereas the currently attended value subspace was present in the DLPFC and ACC, value comparison with stored cues was absent in these regions (Fig. 5k and Supplementary Figs. 6 and 7). A formal comparison of each of the three correlations of interest (corresponding to those shown in Fig. 5c–e) across the three subregions (Fig. 5k) revealed significantly stronger population encoding in the OFC than the DLPFC (attribute trials: values of cue 2 versus cue 1, P = 0.040; option trials: values of cue 3 versus cue 1, P = 0.067; cue 3 versus cue 2, P = 0.011; z test after Fisher r-to-z transformation) and in the OFC than the ACC (attribute trials: value of cue 2 versus cue 1, P = 0.003; option trials: value of cue 3 versus cue 1, P = 0.0003; cue 3 versus cue 2, P = 0.00013).

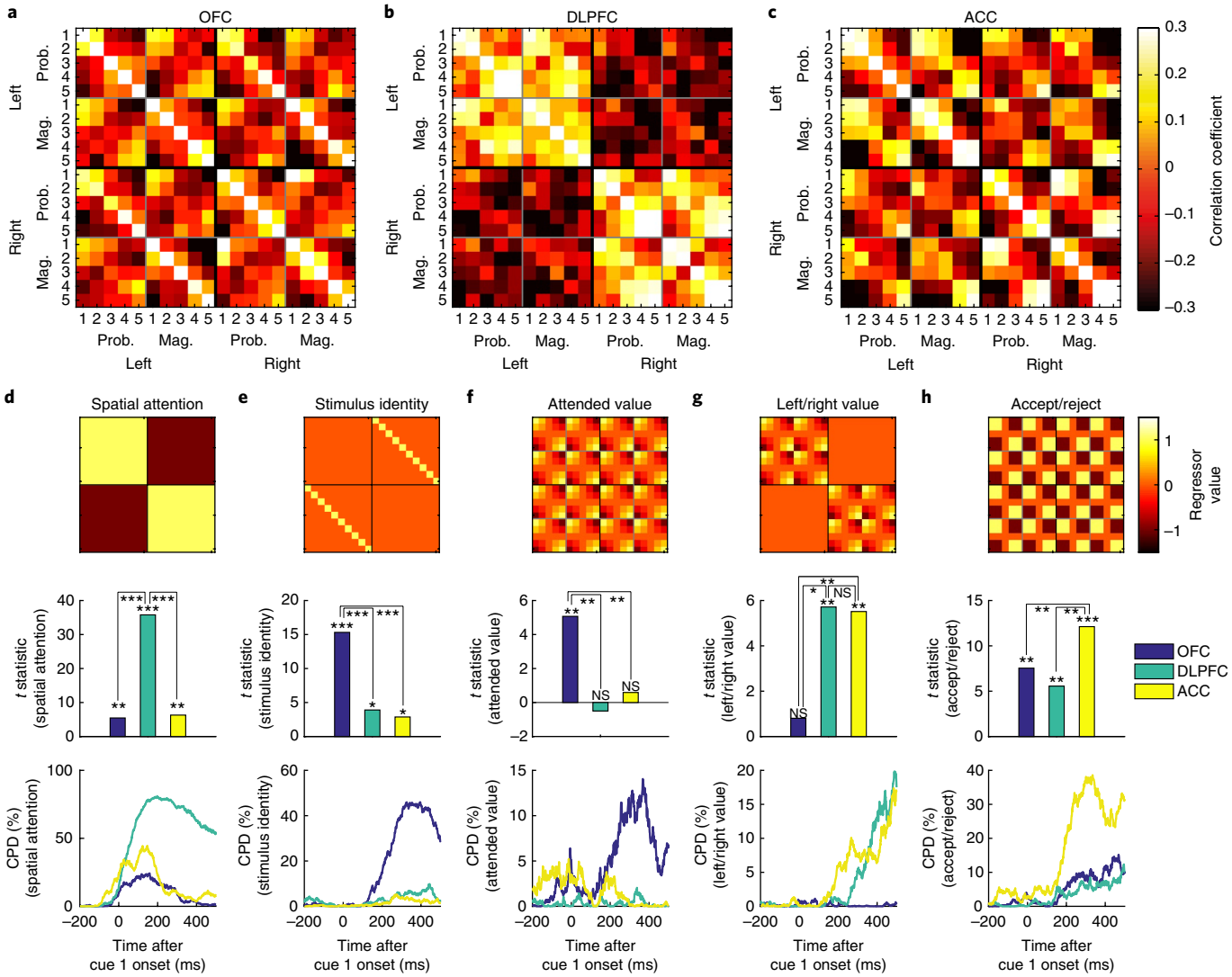

Fig. 4 | Triple dissociation of task-evoked neural codes across OFC, DLPFC and ACC at cue 1 presentation. a, OFC RSA among the ten different cue identities—probability (prob) and magnitude (mag), sorted from the lowest-ranked (1) to highest-ranked (5) picture—when presented in left and right options. For matrix element (*i*,*j*), color denotes the Pearson correlation coefficient of the *z*-scored firing rate between condition *i* and condition *j* across the OFC neuronal population. Firing rates are averaged from 100 ms to 500 ms after stimulus (additional data in Supplementary Video 1). Notably, this matrix collapses across the top/bottom spatial position; 40 × 40 matrix, splitting conditions by spatial position, in Supplementary Fig. 4. **b**,**c**, As in **a**, but for DLPFC (**b**) and ACC populations (**c**). **d**–**h**, Results from multiple linear regression of 'templates' onto RSA matrices. In each column, the template matrix is shown at top, the corresponding regression *t* statistic for each region is shown in the middle, and the coefficient of partial determination from sliding regression of templates onto RSA matrices, with a sliding window of ±100 ms, is shown at bottom. A full description of template matrices, the regression model and statistical inference via nonparametric permutation test can be found in Methods. **d**, The 'spatial attention' template (differentiating cues on the left- versus right-hand options) was particularly prominent in the DLPFC ($t_{399} = 35.782$, $P < 1 \times 10^{-4}$), significantly more so than other regions (one-way analysis of variance (ANOVA) $F_{2,1179} = 311.18$, $P < 1 \times 10^{-4}$; post hoc comparison for DLPFC > ACC, $P < 1 \times 10^{-4}$; post hoc comparison for DLPFC > OFC, $P < 1 \times 10^{-4}$); (**e**), The 'stimulus identity' template (responding similarly to the same cue irrespective of side) was particularly strong in the OFC ($t_{399} = 15.3173$, $P < 1 \times 10^{-4}$), again more so than other regions ($F_{2,1179} = 32.77$, $P < 1 \times 10^{-4}$; post hoc comparisons: OFC > ACC, $P < 1 \times 10^{-4}$; OFC > ACC, $P < 1 \times 10^{-4}$); **f**, The attended-value template (representing the cue 1 value irrespective of stimulus location or attribute) was prominent in the OFC ($t_{399} = 5.0697$, $P = 0.0036$), significantly more so than in other regions ($F_{2,1179} = 6.73$, $P = 0.0126$; post hoc comparisons: OFC > DLPFC, $P = 0.0017$; OFC > ACC: $P = 0.0002$); **g**, The 'left/right value' template was prominent principally within the ACC ($t_{399} = 5.5151$, $P = 0.0096$) and DLPFC ($t_{399} = 5.7156$, $P = 0.0062$), significantly more so than in the OFC ($F_{2,1179} = 9.08$, $P = 0.011$; post hoc comparisons: ACC > OFC, $P = 0.0003$; DLPFC > OFC, $P = 0.011$); **h**, The accept/reject template (reflecting whether cue 1 had high (rank 4 or 5) versus low value (rank 1 or 2)) was strongest in the ACC ($t_{399} = 12.1217$, $P < 1 \times 10^{-4}$), significantly more so than other regions ($F_{2,1179} = 17.20$, $P = 0.0006$; post hoc comparisons: ACC > OFC, $P < 1 \times 10^{-4}$; ACC > DLPFC, $P = 0.0004$). In **d**–**f**, $^{*}P < 0.05$, $^{**}P < 0.005$, $^{***}P < 0.0005$. OFC, $n = 183$ units; DLPFC, $n = 135$ units; ACC, $n = 189$ units. Additional data in Supplementary Fig. 5.

Parallel ACC signals for belief confirmation, choice commitment and action selection. We then evaluated the ACC population activity across cues 2 and 3, on the basis of our earlier interpretation that Fig. 4h might represent a belief-confirmation signal for accepting or rejecting the foreground (current best) option. To test this hypothesis more rigorously, we included four regressors in our regression model that captured belief confirmation at subsequent cues, in both option and attribute trials. When the evidence

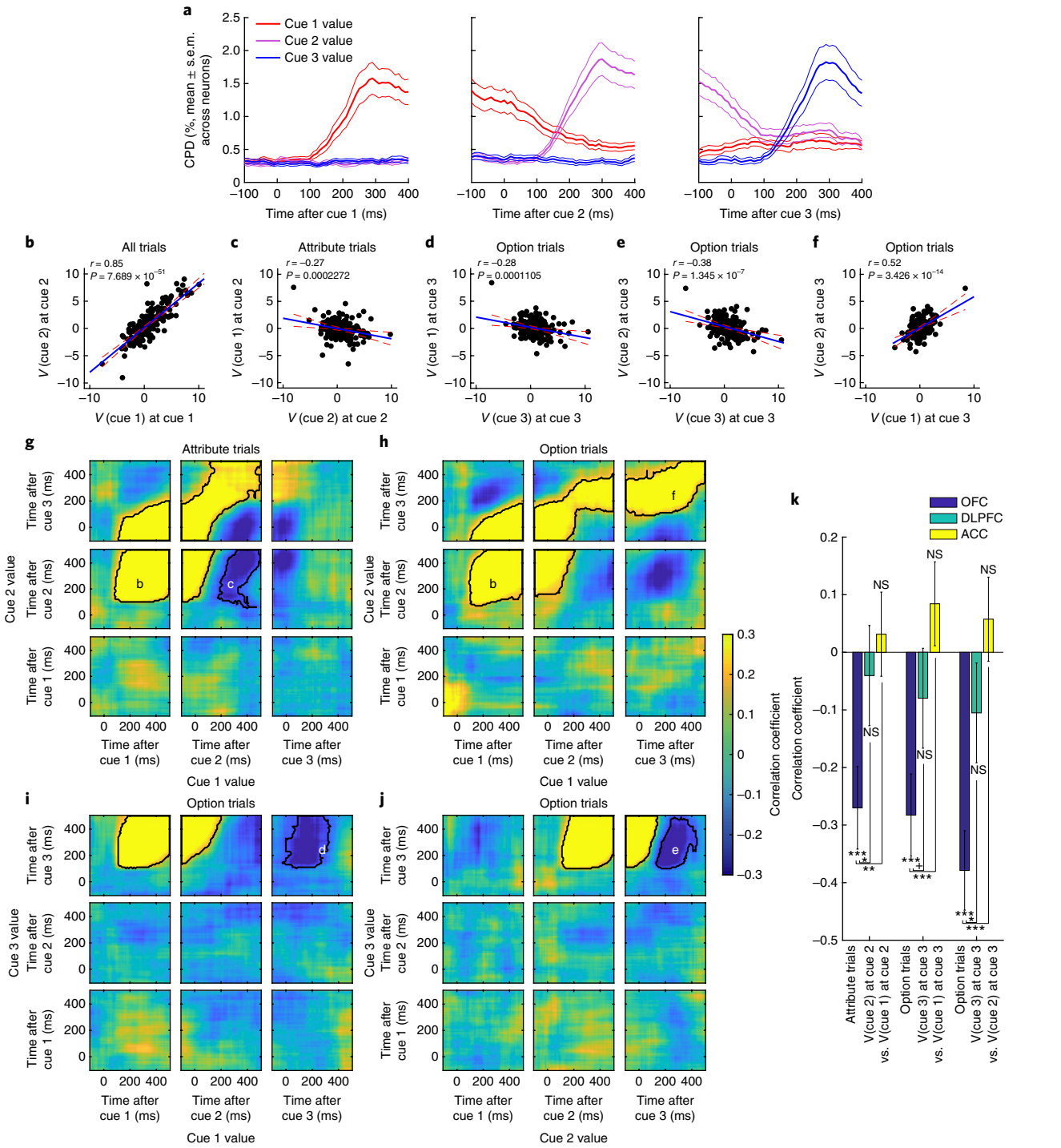

Fig. 5 | Valuation subspaces for attended ('online') and stored cues, supporting attention-guided value comparison in the OFC. a, Coefficient of partial determination for cue 1 value, cue 2 value and cue 3 value, which were time-locked to each cue's presentation with a sliding 200-ms window. Lines denote mean ± s.e.m. across neurons. **b**, Positive relationship between *t* statistics from the regression of the value (*V*) of cue 1 when cue 1 is presented (ordinate), and the value of cue 2 when cue 2 is presented (abscissa), thus suggesting a stable subspace reflecting the currently attended value. **c**, When cue 2 is being attended to in attribute trials, the online value subspace (ordinate) correlates negatively with the subspace reflecting the stored value of cue 1 (abscissa). **d–f**, When cue 3 is being attended to in option trials, the attended value subspace (ordinates of **d** and **e**) correlates negatively with the subspace for stored values of both cue 1 (abscissa of **d**) and cue 2 (abscissa of **e**). The two stored subspaces are positively correlated (**f**). **g–j**, Cross-correlation matrices reflecting the time-varying relationship among different value subspaces in attribute trials (in **g**) and option trials (in **h–j**). Heat maps reflect the correlation coefficient between *t* statistics from regression for each cue's value across the OFC population. Superimposed letters refer to the correlations plotted above, in **b–f**. Black lines denote significant clusters ($P < 0.001$, cluster-based permutation test, corrected for multiple comparisons). **k**, Negative correlations in **c–e** are present in only the OFC and are significantly stronger in the OFC ($n = 183$ units) than the DLPFC ($n = 135$ units) and ACC ($n = 189$ units); bars show correlation coefficient ± s.e. (NS, nonsignificant, $^{***}P < 0.001$, $^{**}P < 0.01$, $^{*}P < 0.05$ (two-tailed), $^{+}P < 0.05$ (one-tailed), Fisher's *r*-to-*z* transform). Correlations in **b–f** and **k** are defined with a window of 150–350 ms after stimulus onset. All correlation coefficients were determined with Pearson's correlation. Additional data are shown in Supplementary Figs. 6 and 7.

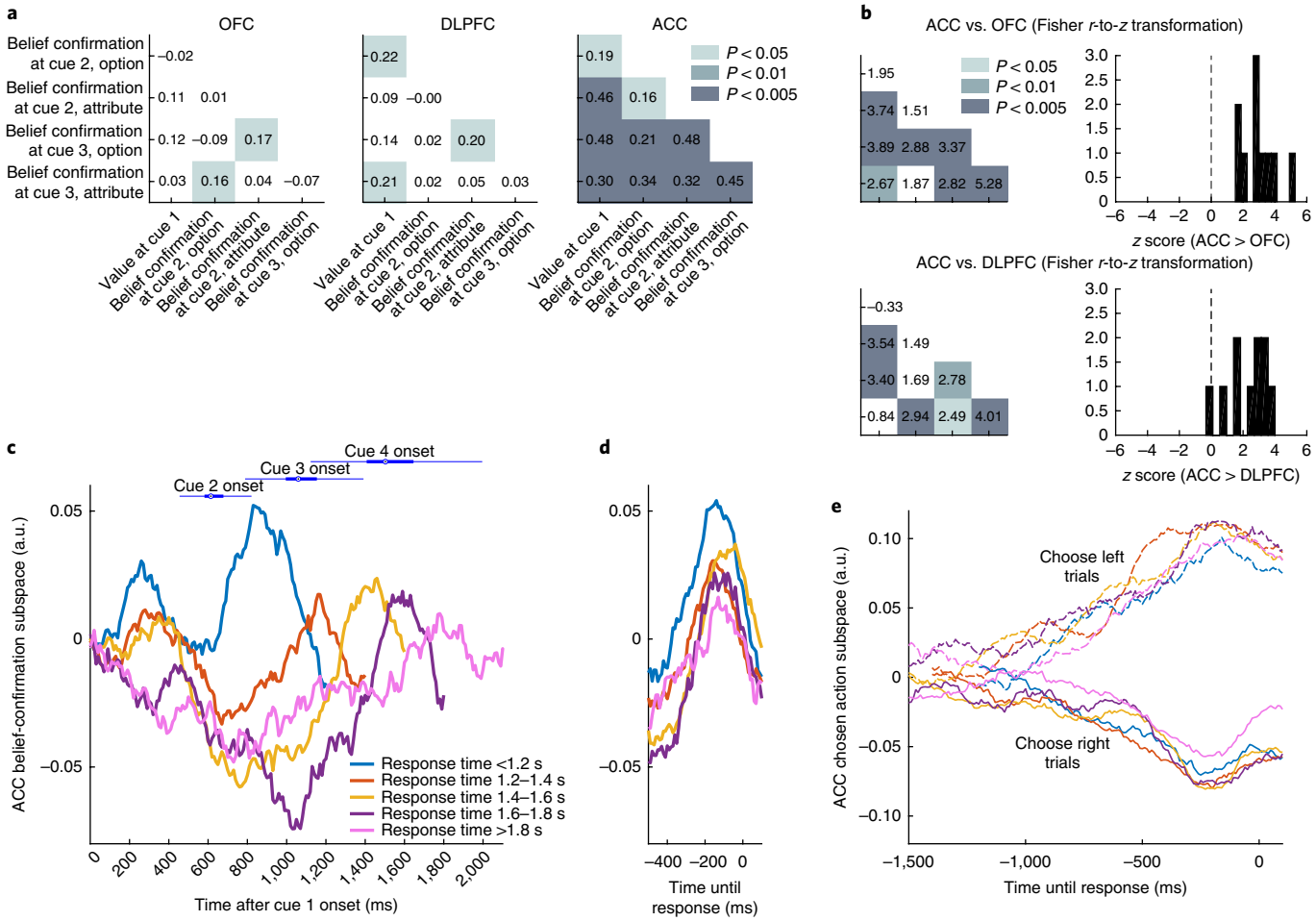

Fig. 6 | Multiple signals in the ACC reflect belief confirmation, commitment to a course of action and accumulation of evidence for left/right movement. **a**, Positive population correlations among four orthogonal regressors that reflect belief confirmation at cue 2/cue 3 in both option and attribute trials (cf. Supplementary Fig. 8), and initial-value population response at cue 1 (cf. Fig. 4h), thus demonstrating a stable belief-confirmation subspace in the ACC ($n = 189$ units) across multiple cues. The value inside each box denotes the Pearson correlation of parameter estimates across the neural population in each region; shading denotes significance. Individual ACC correlations are shown in Supplementary Fig. 10. **b**, Formal comparison of correlations shown in a, determined with Fisher's *r*-to-*z* transformation against the OFC ($n = 183$ units) and DLPFC ($n = 135$ units). Left, individual *z* scores/significance for each comparison (same layout as in **a**). Right, distribution of *z* scores. **c**,**d**, Projecting ACC population activity into the belief-confirmation subspace reveals ramping immediately before the commitment to joystick movement. A.u., arbitrary units. In **c**, trials are sorted by response time and time-locked to the cue 1 onset (blue bars above are box plots of cue onset times for other cues). For box plots, center line, median; box limits, upper and lower quartiles; whiskers, extreme values. In **d**, trials are time-locked to response onset. **e**, An orthogonal subspace in the ACC reflects the emergence of an action plan to choose the left or the right option. Activity in this subspace progressively favors one action over the other over time. The relationship between belief confirmation and action selection subspaces is shown in Supplementary Video 2.

presented thus far suggested that the currently attended side should be chosen, we hypothesized that belief confirmation would scale positively with the currently attended value. In contrast, when the evidence suggested that the unattended side should be chosen, we hypothesized that belief confirmation would scale negatively with value (Supplementary Fig. 8). As a consequence, all four belief-confirmation regressors were by definition orthogonal to the currently attended value (Supplementary Fig. 9).

We used these regressors to test whether the ACC reliably encoded belief confirmation and found that the ACC-population subspaces for each of these regressors significantly correlated with one another and also with cue 1 belief confirmation (Fig. 6a and Supplementary Fig. 10). Because all five regressors were defined at different parts of the trial, the results revealed a stable population code in the ACC for accepting/rejecting the current belief, which was not present in the OFC or DLPFC (Fig. 6a). We again formally compared the correlations among these regressors across subregions, by using a Fisher *r*-to-*z* transformation (Fig. 6b). Virtually all of these correlations were stronger in the ACC than the OFC/DLPFC (Fig. 6b, right), and most individual comparisons were significant (Fig. 6b, left).

We next asked whether this belief-confirmation subspace in the ACC might support commitment to a final decision[12,15]. To answer this question, we examined the temporal evolution of belief-confirmation-subspace activity, by using the regressors in Supplementary Fig. 8 and Fig. 6a. We used one-half of all trials to define the subspace and projected the data from the remaining half into that subspace to examine its evolution across time. To ensure statistical robustness, we repeated this procedure by using 100 random splits of the data to obtain a distribution of these projection results, then averaged across this distribution. Positive values on the ordinate in Fig. 6c,d thus indicated more activity in the subspace aligned with the 'belief confirmation' regressors in Supplementary Fig. 8.

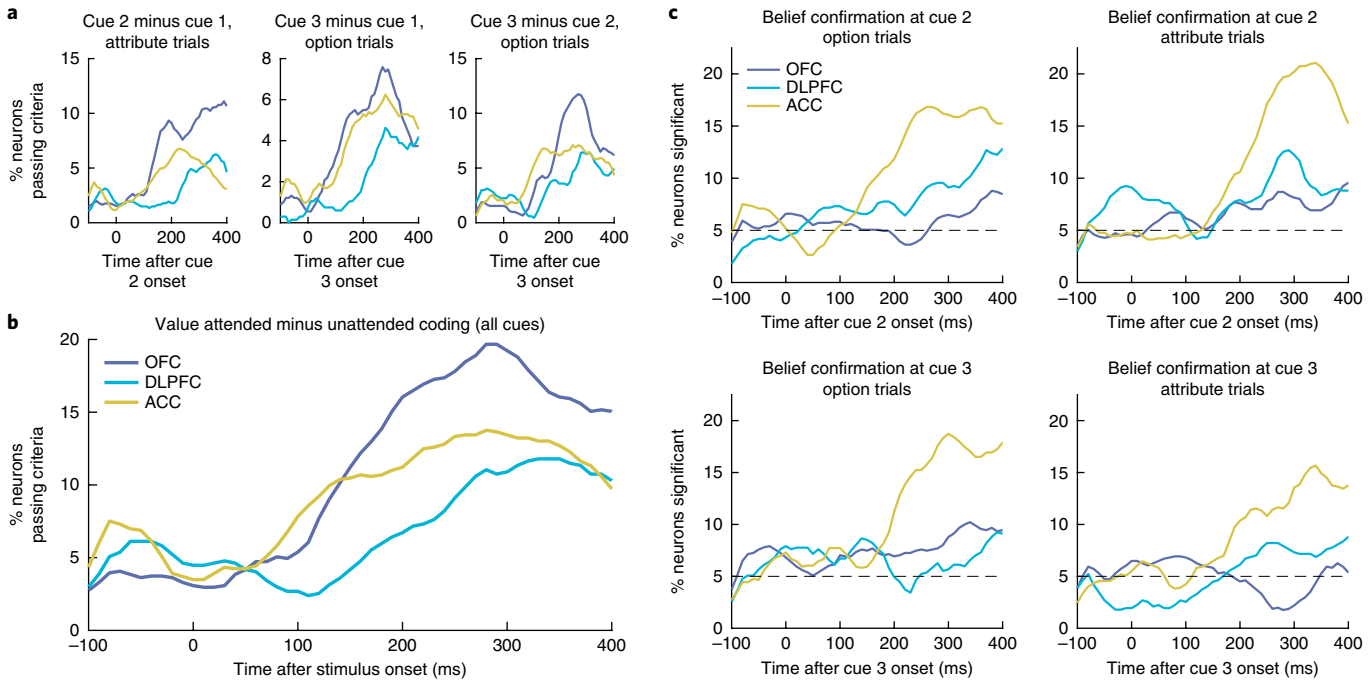

Fig. 7 | Single-neuron analysis of attention-guided value comparison and belief confirmation recapitulates findings of population analysis. a, Attention-guided value comparison can be defined by using three separate epochs and sets of regressors (details in main text). All three definitions show a greater proportion on neurons significantly encoding attention-guided value comparison in the OFC ($n=183$ units) than in the DLPFC ($n=135$ units) or ACC ($n=189$ units). **b**, Percentage of neurons that encoded value attended minus value unattended across any of the three different epochs in **a**. **c**, There are four separate ways of defining belief confirmation (details in main text and Supplementary Fig. 8). All four definitions show a greater proportion of neurons significantly encoding belief confirmation in the ACC than the OFC or DLPFC.

Time-varying ACC activity within this subspace showed distinct dynamics in trials of different reaction times (Fig. 6c). First, the activity in this subspace separated short- from long-reaction-time trials relatively early during the course of making a choice, even at the time of cue 1 presentation. One interpretation of this finding is that the first attended item is initially referenced as the 'default' option to be accepted or rejected, and evidence is interpreted either in favor of or against this default[34]. Confirmatory evidence may lead to executing a final choice more rapidly (Fig. 2b), with faster reaction times in these trials. Second, irrespective of reaction time, ACC activity ramped shortly before joystick movement (Fig. 6d). Activity within the belief-confirmation subspace therefore became prominent immediately before commitment to action, in all trials.

Finally, we found that the ACC contains a signal relevant to which action is selected (Fig. 4g), in agreement with previous results[12,13,15,42]. We defined a separate subspace for whether the subject would choose left or right in the current trial, adopting the same split-half approach as in Fig. 6c,d. Activity in the ACC action-selection subspace also gradually ramped as evidence was revealed about which option to choose and peaked immediately before action selection (Fig. 6e). Belief-confirmation and action-selection subspaces are orthogonal; the relationship between them can be seen in Supplementary Video 2.

Single-neuron analyses recapitulate core findings at the population level. The analyses in Figs. 4–6 explored how information is represented at the level of the neural ensemble rather than at the level of the single neuron. This procedure exploits the known heterogeneity of PFC single-neuron responses[14,15,17,36,40,42] to study task representations distributed across a population of cells. There is a strong theoretical and empirical foundation supporting the study of information representation at the population level[43], which has motivated several recent studies of PFC neuronal responses[10,18,21,41]. However, much of the previous literature has emphasized information representation at the level of single neurons. To facilitate comparison with this literature, we examined whether there were differences among PFC subregions in the fraction of neurons selective for key variables at different stages of the task. The results of these analyses recapitulated the core findings at the population level.

We first tested whether the OFC had more neurons encoding value comparison between currently and previously attended stimuli than other subregions. We performed three analyses analogous to those in Fig. 5c–e. At cue 2 in attribute trials (cf. Fig. 5c), we asked whether neurons encoded a value difference between cue 2 and cue 1; at cue 3 in option trials, we asked whether they encoded a value difference between cue 3 and cue 1 (cf. Fig. 5d); at the same time point, we asked whether neurons encoded a value difference between cue 3 and cue 2 (cf. Fig. 5e). To consider a neuron as representing value difference, we required that the contrast of parameter estimates (i.e., (value attended) – (value unattended)) be significant and also that (value attended) and (value unattended) be independently significant with opposing signs. At all three relevant time points, we found that a greater proportion of single neurons passed these criteria in the OFC than in the ACC and DLPFC (Fig. 7a). We collapsed data across these three tests to show the fraction of single neurons passing these criteria at any of the three cues individually (Fig. 7b).

We next tested whether the ACC had a larger proportion of neurons encoding belief confirmation than other subregions. Here, we asked whether each neuron significantly encoded the four regressors depicted in Supplementary Fig. 8, corresponding to belief confirmation at cue 2 or 3 in option or attribute trials. These were the four regressors whose parameter estimates correlated with one another in the ACC (Supplementary Fig. 10) but not the OFC or

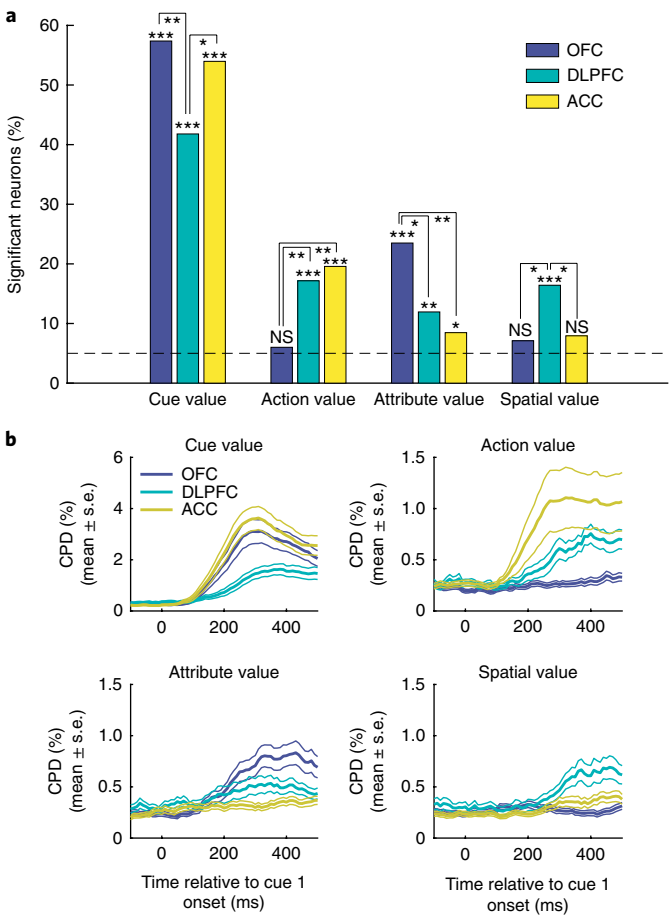

Fig. 8 | Single-neuron correlates of task variables at cue 1 presentation. a, Fractions of ACC ($n=189$ units), DLPFC ($n=135$ units) and OFC ($n=183$ units) neurons significantly encoding cue value, action value (left minus right), attribute value (probability minus magnitude) and spatial value (top minus bottom) in firing rates 100–500 ms after cue 1 onset. Significance denotes two-sided binomial test against chance encoding (5%) for each bar (cue value: ACC, $P<1\times10^{-5}$, DLPFC, $P<1\times10^{-5}$, OFC, $P<1\times10^{-5}$; action value: ACC, $P<1\times10^{-5}$, DLPFC, $P<1\times10^{-5}$, OFC, $P=0.4139$; attribute value: ACC, $P=0.029$, DLPFC, $P=0.0023$, OFC, $P<1\times10^{-5}$; spatial value: ACC, $P=0.0572$, DLPFC, $P<1\times10^{-5}$, OFC, $P=0.0845$), and pairwise chi square tests for comparisons between regions; NS, nonsignificant; *$P<0.05$, ** $P<0.01$, *** $P<0.001$. **b**, Coefficient of partial determination estimated in sliding 200-ms bins for cue, action, attribute and spatial value in each region (mean ± s.e. across neurons).

DLPFC (Fig. 6a), and formed the 'belief-confirmation subspace' shown in Fig. 6c,d. At all four time points, there was a greater proportion of single neurons significantly encoding belief confirmation in the ACC than in the OFC or DLPFC (Fig. 7c).

Finally, we performed an additional regression analysis at cue 1 onset to examine how factors relating to the values of different task features were represented in PFC. We again capitalized on the ability of each cue to be decomposed into multiple features: associated action, attribute, spatial position and value. These different values were entered into the same regression model, thus allowing us to test the unique contribution of each of these features in explaining variance in neuronal firing across different regions. Across all three regions, a significant fraction of neurons encoded cue 1's value, irrespective of the cue's attribute, action or spatial position (Fig. 8; binomial test, all $P<1\times10^{7}$). We also found that single neurons encoded value in distinct frames of reference across PFC subregions.

First, a significant subset of ACC and DLPFC neurons (~18%) preferentially responded to the values of either left or right options (binomial test, both $P<1\times10^{-5}$). Both of these populations were significantly greater than the OFC population, which encoded action value at chance level (pairwise chi square test, ACC versus OFC, $P=0.002$; DLPFC versus OFC, $P=0.003$). The time course of these signals (Fig. 8b) was similar to that identified in the population analysis of cue 1 activity through RSA (Fig. 4f,g).

Because left and right options were spatially dissociated, ACC and DLPFC neurons might encode value with reference to various spatial locations (as opposed to action). However, in a region tuned to spatial location rather than action, one would also expect to find neurons that differentiate value for cues in the top part of the visual display compared with the bottom part. In DLPFC, such a relationship held: the populations of top–bottom 'spatial value' neurons and left–right 'action value' neurons were equally prevalent (binomial test, $P<1\times10^{-6}$). In the ACC, this population was significantly smaller than the left–right value population (pairwise chi square test $P=0.03$). In agreement with its strong modulation by attention in Fig. 4a, this result suggests that DLPFC preferentially encodes value in the reference frame of spatial position, whereas the ACC encodes value with respect to relevant choice actions.

Finally, replicating previous results[44], we found that a significant proportion of neurons in the OFC (~24%) reflected attribute value (binomial test, $P<1\times10^{7}$): the neurons preferentially responded to the values of cues for either probability or magnitude. This proportion was significantly greater than the representation of attribute-value coding in either the ACC or DLPFC (pairwise chi square tests, OFC versus ACC, $P=0.001$; OFC versus DLPFC, $P=0.014$). We interpret this finding with a degree of caution, however. OFC neurons might potentially appear to reflect attribute value as an artifact of being particularly selective for individual stimulus identities (RSA, Fig. 4a,e; example neuron, Supplementary Fig. 3b). There was no clear RSA evidence for attribute-specific value coding in the OFC (Fig. 4a).

Discussion

In real-world decision tasks, value-guided decision-making is heavily influenced by visual attention. Information-gathering strategies of both human consumers[22–24,27] and foraging animals[45] have been well characterized as constituting consecutive consideration of each choice option and its component attributes. Our findings demonstrate that as attention is first deployed to a choice option, population codes for decision-related processes emerge simultaneously rather than sequentially in the ACC, OFC and DLPFC (Figs. 4 and 8), thus strongly supporting distributed and parallel models of value-based choice[7,8]. As attention was redeployed to sample further information, the OFC activity reflected an attention-guided value comparison (Figs. 5 and 7), whereas the ACC activity reflected belief updating in light of new evidence and commitment to a final action (Figs. 6 and 7).

In addition to providing functional dissociations across PFC subregions, our paradigm allowed us to explore subjects' information-sampling behavior, which suggested how the subjects might be solving the task. In particular, the subjects were biased toward sampling information from an option that they currently intended to choose (Fig. 2a), even when that information would yield little or no information about the choice (Fig. 2b). This finding mirrors biases that we have recently observed in a version of the same experiment in humans[25] and is consistent with monkeys' willingness to sacrifice reward to obtain information about reward delivery[46]. Such behaviors could be interpreted of in terms of a mechanism for solving the value-based choice of having a foreground option in mind and deciding sequentially whether to accept or reject that option relative to alternatives[8].

An accept/reject strategy for value-based choice might be considered quite natural in the broader context of the real-world

foraging decisions faced by our evolutionary ancestors[31]. These strategies are inherently sequential in nature and involve decisions such as whether to accept or reject a current patch. Such patch-leaving decisions rely on ramping signals in the ACC before action selection[20,47]. In our task, the ACC categorized the first-attended option nonlinearly into cues that might be accepted or rejected (Fig. 4c,h); had a stable belief-confirmation code for accepting/rejecting the foreground option in light of new evidence (Fig. 6a and Supplementary Figs. 8 and 10); and integrated that evidence toward a decision bound (Fig. 6c,d) while signaling which action would be chosen (Fig. 6e). There are a number of seemingly discrepant accounts of ACC function, such as its role in value updating[3,5,14], action–outcome prediction[13], information seeking[21], behavioral adaptation[18,20,47] and action selection[5,15,42]. The computations that we identified in the ACC are consistent with these accounts but occurred at distinct time points or within orthogonal subspaces (Supplementary Video 2), thereby reconciling some of the outstanding debate concerning ACC function.

In contrast, the OFC initially carried a representation of the identity and value of the first-attended stimulus, in agreement with its anatomical projections from regions of the inferotemporal cortex[48] representing highly processed visual information such as object identity[49]. As further information was attended to, simultaneous coding of attended and stored information emerged uniquely in OFC populations (Fig. 5) and provided a relative value-coding mechanism for how choice options are compared. Such attention-guided relative value-coding mechanisms form a central component of value comparison in recent accept/reject models of economic choice[31], as well as other decision models[24]. Our findings are consistent with similar findings in the adjacent ventromedial prefrontal cortex[9,10] but extend these results in important ways. For example, in option trials, we observed how the OFC neural ensemble combines the value associated with multiple components of an option. Attribute integration did not occur immediately after the second cue was attended to but instead occurred only after the third cue was attended to in the alternative option (Fig. 5f,h) and value comparison could take place (Fig. 5d,e,i,j). Our findings also indicate that with respect to attended stimuli, attention-guided value comparison is neuroanatomically specific (cf. Supplementary Figs. 6 and 7). We note, however, that value comparison may still be supported in other structures in complementary frames of reference[7,8], for instance in the space of action value in the ACC (Fig. 4g).

An important caveat of our study is that our analyses were based on pseudoensembles, not large ensembles of simultaneously recorded neurons. We typically isolated between 5 and 25 single units per recording session (Supplementary Table 1). Further insight into the relationships among different PFC subregions' decision dynamics might be obtained with higher-yield simultaneous population-recording techniques.

In summary, theoretical models suggest that decision-making requires several computations including stimulus identification, valuation and integration with other attributes, in comparison to previous choice options and action selection[7,8,50]. More recently, value-based decision-making has been suggested to be linked to other forms of choice such as sequential foraging decisions[8,31]. Although value-related signals are commonly found in the PFC, a mechanistic account describing how distinct PFC subregions contribute to these computations has been lacking. Using a naturalistic information search and decision task that afforded exploration of how decision-related computations evolve as evidence informing choice is attended to, we isolated these computations dissociably across PFC subregions. Our results therefore provide a unifying account of how PFC subregions support value-guided choice.

Received: 15 December 2017; Accepted: 11 August 2018;
Published online: 26 September 2018

References

1. Yeterian, E. H., Pandya, D. N., Tomaiuolo, F. & Petrides, M. The cortical connectivity of the prefrontal cortex in the monkey brain. *Cortex* **48**, 58–81 (2012).
2. Haber, S. N. & Behrens, T. E. J. The neural network underlying incentive-based learning: implications for interpreting circuit disruptions in psychiatric disorders. *Neuron* **83**, 1019–1039 (2014).
3. Rushworth, M. F. S., Noonan, M. P., Boorman, E. D., Walton, M. E. & Behrens, T. E. Frontal cortex and reward-guided learning and decision-making. *Neuron* **70**, 1054–1069 (2011).
4. Donoso, M., Collins, A. G. & Koechlin, E. Foundations of human reasoning in the prefrontal cortex. *Science* **344**, 1481–1486 (2014).
5. Rudebeck, P. H. et al. Frontal cortex subregions play distinct roles in choices between actions and stimuli. *J. Neurosci.* **28**, 13775–13785 (2008).
6. Vaidya, A. R. & Fellows, L. K. Testing necessary regional frontal contributions to value assessment and fixation-based updating. *Nat. Commun.* **6**, 10120 (2015).
7. Cisek, P. Making decisions through a distributed consensus. *Curr. Opin. Neurobiol.* **22**, 927–936 (2012).
8. Hunt, L. T. & Hayden, B. Y. A distributed, hierarchical and recurrent framework for reward-based choice. *Nat. Rev. Neurosci.* **18**, 172–182 (2017).
9. Lim, S. L., O'Doherty, J. P. & Rangel, A. The decision value computations in the vmPFC and striatum use a relative value code that is guided by visual attention. *J. Neurosci.* **31**, 13214–13223 (2011).
10. Strait, C. E., Blanchard, T. C. & Hayden, B. Y. Reward value comparison via mutual inhibition in ventromedial prefrontal cortex. *Neuron* **82**, 1357–1366 (2014).
11. McGinty, V. B., Rangel, A. & Newsome, W. T. Orbitofrontal cortex value signals depend on fixation location during free viewing. *Neuron* **90**, 1299–1311 (2016).
12. Hare, T. A., Schultz, W., Camerer, C. F., O'Doherty, J. P. & Rangel, A. Transformation of stimulus value signals into motor commands during simple choice. *Proc. Natl. Acad. Sci. USA* **108**, 18120–18125 (2011).
13. Alexander, W. H. & Brown, J. W. Medial prefrontal cortex as an action-outcome predictor. *Nat. Neurosci.* **14**, 1338–1344 (2011).
14. Kennerley, S. W., Behrens, T. E. J. & Wallis, J. D. Double dissociation of value computations in orbitofrontal and anterior cingulate neurons. *Nat. Neurosci.* **14**, 1581–1589 (2011).
15. Cai, X. & Padoa-Schioppa, C. Neuronal encoding of subjective value in dorsal and ventral anterior cingulate cortex. *J. Neurosci.* **32**, 3791–3808 (2012).
16. Behrens, T. E., Woolrich, M. W., Walton, M. E. & Rushworth, M. F. Learning the value of information in an uncertain world. *Nat. Neurosci.* **10**, 1214–1221 (2007).
17. Bernacchia, A., Seo, H., Lee, D. & Wang, X. J. A reservoir of time constants for memory traces in cortical neurons. *Nat. Neurosci.* **14**, 366–372 (2011).
18. Karlsson, M. P., Tervo, D. G. R. & Karpova, A. Y. Network resets in medial prefrontal cortex mark the onset of behavioral uncertainty. *Science* **338**, 135–139 (2012).
19. Bryden, D. W., Johnson, E. E., Tobia, S. C., Kashtelyan, V. & Roesch, M. R. Attention for learning signals in anterior cingulate cortex. *J. Neurosci.* **31**, 18266–18274 (2011).
20. Hayden, B. Y., Pearson, J. M. & Platt, M. L. Neuronal basis of sequential foraging decisions in a patchy environment. *Nat. Neurosci.* **14**, 933–939 (2011).
21. Stoll, F. M., Fontanier, V. & Procyk, E. Specific frontal neural dynamics contribute to decisions to check. *Nat. Commun.* **7**, 11990 (2016).
22. Payne, J. W. Task complexity and contingent processing in decision-making - information search and protocol analysis. *Organ. Behav. Hum. Perform.* **16**, 366–387 (1976).
23. Bettman, J. R., Luce, M. F. & Payne, J. W. Constructive consumer choice processes. *J. Consum. Res.* **25**, 187–217 (1998).
24. Krajbich, I., Armel, C. & Rangel, A. Visual fixations and the computation and comparison of value in simple choice. *Nat. Neurosci.* **13**, 1292–1298 (2010).
25. Hunt, L. T., Rutledge, R. B., Malalasekera, W. M. N., Kennerley, S. W. & Dolan, R. J. Approach-induced biases in human information sampling. *PLoS Biol.* **14**, e2000638 (2016).
26. Stewart, N., Hermens, F. & Matthews, W. J. Eye movements in risky choice. *J. Behav. Decis. Mak.* **29**, 116–136 (2016).
27. Gidlof, K., Wallin, A., Dewhurst, R. & Holmqvist, K. Using eye tracking to trace a cognitive process: gaze behaviour during decision making in a natural environment. *J. Eye Mov. Res.* **6**, 1–14 (2013).
28. Daddaoua, N., Lopes, M. & Gottlieb, J. Intrinsically motivated oculomotor exploration guided by uncertainty reduction and conditioned reinforcement in non-human primates. *Sci. Rep.* **6**, 20202 (2016).
29. Passingham, R.E. & Wise, S.P. in *The Neurobiology of the PrefrontalCortex*. Ch. 2, 26–64 (Oxford University Press, Oxford, 2012).
30. Gottlieb, J., Hayhoe, M., Hikosaka, O. & Rangel, A. Attention, reward, and information seeking. *J. Neurosci.* **34**, 15497–15504 (2014).

31. Hayden, B. Y. Economic choice: the foraging perspective. *Curr. Opin. Behav. Sci.* **24**, 1–6 (2018).
32. Fellows, L. K. Deciding how to decide: ventromedial frontal lobe damage affects information acquisition in multi-attribute decision making. *Brain* **129**, 944–952 (2006).
33. Nickerson, R. S. Confirmation bias: a ubiquitous phenomenon in many guises. *Rev. Gen. Psychol.* **2**, 175–220 (1998).
34. Boorman, E. D., Rushworth, M. F. & Behrens, T. E. Ventromedial prefrontal and anterior cingulate cortex adopt choice and default reference frames during sequential multi-alternative choice. *J. Neurosci.* **33**, 2242–2253 (2013).
35. Wittmann, M. K. et al. Predictive decision making driven by multiple time-linked reward representations in the anterior cingulate cortex. *Nat. Commun.* **7**, 12327 (2016).
36. Kaping, D., Vinck, M., Hutchison, R. M., Everling, S. & Womelsdorf, T. Specific contributions of ventromedial, anterior cingulate, and lateral prefrontal cortex for attentional selection and stimulus valuation. *PLoS Biol.* **9**, e1001224 (2011).
37. Kriegeskorte, N., Mur, M. & Bandettini, P. Representational similarity analysis: connecting the branches of systems neuroscience. *Front. Syst. Neurosci.* **2**, 4 (2008).
38. Rich, E. L. & Wallis, J. D. Decoding subjective decisions from orbitofrontal cortex. *Nat. Neurosci.* **19**, 973–980 (2016).
39. Hunt, L. T., Behrens, T. E., Hosokawa, T., Wallis, J. D. & Kennerley, S. W. Capturing the temporal evolution of choice across prefrontal cortex. *eLife* **4**, e11945 (2015).
40. Cai, X., Kim, S. & Lee, D. Heterogeneous coding of temporally discounted values in the dorsal and ventral striatum during intertemporal choice. *Neuron* **69**, 170–182 (2011).
41. Mante, V., Sussillo, D., Shenoy, K. V. & Newsome, W. T. Context-dependent computation by recurrent dynamics in prefrontal cortex. *Nature* **503**, 78–84 (2013).
42. Kennerley, S. W., Dahmubed, A. F., Lara, A. H. & Wallis, J. D. Neurons in the frontal lobe encode the value of multiple decision variables. *J. Cogn. Neurosci.* **21**, 1162–1178 (2009).
43. Yuste, R. From the neuron doctrine to neural networks. *Nat. Rev. Neurosci.* **16**, 487–497 (2015).
44. O'Neill, M. & Schultz, W. Coding of reward risk by orbitofrontal neurons is mostly distinct from coding of reward value. *Neuron* **68**, 789–800 (2010).
45. O'Brien, W. J., Browman, H. I. & Evans, B. I. Search strategies of foraging animals. *Am. Sci.* **78**, 152–160 (1990).
46. Blanchard, T. C., Hayden, B. Y. & Bromberg-Martin, E. S. Orbitofrontal cortex uses distinct codes for different choice attributes in decisions motivated by curiosity. *Neuron* **85**, 602–614 (2015).
47. Kolling, N., Behrens, T., Wittmann, M. K. & Rushworth, M. Multiple signals in anterior cingulate cortex. *Curr. Opin. Neurobiol.* **37**, 36–43 (2016).
48. Cavada, C., Compañy, T., Tejedor, J., Cruz-Rizzolo, R. J. & Reinoso-Suárez, F. The anatomical connections of the macaque monkey orbitofrontal cortex: a review. *Cereb. Cortex* **10**, 220–242 (2000).
49. DiCarlo, J. J., Zoccolan, D. & Rust, N. C. How does the brain solve visual object recognition? *Neuron* **73**, 415–434 (2012).
50. Padoa-Schioppa, C. Neurobiology of economic choice: a good-based model. *Annu. Rev. Neurosci.* **34**, 333–359 (2011).

Acknowledgements

L.T.H. was supported by a Henry Wellcome Fellowship (098830/Z/12/Z) and Henry Dale Fellowship (208789/Z/17/Z) from the Wellcome Trust; a NARSAD Young Investigator Grant from the Brain and Behavior Research Foundation; and the NIHR Oxford Health Biomedical Research Centre. W.M.N.M. was supported by funding from the Astor Foundation, Rosetrees Trust and Middlesex Hospital Medical School General Charitable Trust. A.O.d.B. was supported by a PhD studentship from the MRC. B.M. was supported by the Fundação para a Ciência e Tecnologia (scholarship SFRH/BD/51711/2011). T.E.J.B. was supported by a Wellcome Trust Senior Research Fellowship (WT104765MA) and funding from the James S. McDonnell Foundation (JSMF220020372). S.W.K. was supported by a Wellcome Trust New Investigator Award (096689/Z/11/Z). The views expressed are those of the authors and are not necessarily those of the NHS, the NIHR or the Department of Health.

Author contributions

L.T.H. designed experiments, collected and analyzed data and wrote the manuscript; W.M.N.M. designed experiments and collected and analyzed data; A.O.d.B. analyzed data; B.M. collected data; S.F.F. designed experiments; T.E.J.B. designed experiments and supervised analysis; S.W.K. supervised all aspects of the project and wrote the manuscript.

Competing interests

The authors declare no competing interests.

Additional information

Supplementary information is available for this paper at https://doi.org/10.1038/s41593-018-0239-5.

Reprints and permissions information is available at www.nature.com/reprints.

Correspondence and requests for materials should be addressed to L.T.H. or S.W.K.

Publisher's note: Springer Nature remains neutral with regard to jurisdictional claims in published maps and institutional affiliations.

Methods

Subjects. Two adult male rhesus monkeys (*M. mulatta*), subjects M and F, were used. The subjects weighed 7–10 kg at the time of neuronal data collection, and both were ~4 years old at the start of the experiment. We regulated their daily fluid intake to maintain motivation in the task. All experimental procedures were approved by the UCL Local Ethical Procedures Committee and the UK Home Office, and carried out in accordance with the UK Animals (Scientific Procedures) Act.

Behavioral protocol. Subjects sat with their heads restrained in a behavioral chair facing a 19-inch computer monitor placed approximately 57 cm away from the subjects' eyes. The height of the screen was adjusted so that the center of the screen aligned with neutral eye level for the subject. A voltage-gating joystick (APEM Components) was placed in front of the subject out of the line of sight and was used to make manual responses during the task. Eye position and pupil tracking were achieved with an infrared camera (ISCAN ETL-200) sampled at 240 Hz. The behavioral paradigm was run in the MATLAB-based toolbox MonkeyLogic (http://www.monkeylogic.net/, Brown University)[51–53]. All joystick and eye positions were relayed to MonkeyLogic for use online during the task and were also recorded by MonkeyLogic at 1,000 Hz. Juice delivery was achieved by using a precision peristaltic pump (ISMATEC IPC) to deliver juice to a spout placed at the lips of the subject. Subject M was given dilute (50%) apple juice, and subject F was given dilute (50%) mango juice.

Subjects were taught the value of a set of ten isoluminant picture cues pertaining to either magnitude or probability value (further details in 'Task' below) by using secondary conditioning on a separate day before data acquisition. This set of cues was then used for the following one to four recording sessions, at which point a new set of cues was taught to the subject. In total, subject M learned 13 separate sets of cues, and subject F learned 11 sets.

Task. A representation of the task structure is shown in Fig. 1a. Subjects initiated the trial by maintaining saccadic fixation on the center of the screen and central fixation of the joystick for 500 ms. After this fixation was achieved, two options were presented on the screen (left and right of center). Each option consisted of two prelearned picture cues assigned to two different value attributes: probability of reward (10%, 30%, 50%, 70% or 90%) and magnitude of juice reward (0.15 AU, 0.35 AU, 0.55 AU, 0.75 AU or 0.95 AU). The cues were uniformly sampled (with replacement, i.e., sometimes the same cue appeared in both options). The reward magnitude (volume) was varied by manipulation of the length of time that a reward pump was driven, and the absolute values (i.e., reward time) associated with each stimulus varied slightly between subjects. Importantly, all four picture cues were covered up by gray squares with the exception of one, which was covered by a blue square. The blue square informed the subject of the location of a required saccade. After the subject made a saccade and fixated on the blue square, the blue square was replaced by the picture cue, which the subject was required to continuously fixate on for 300 ms. If continuous fixation was not achieved within 1,200 ms, the trial was aborted, and the subject received a short timeout. After this fixation period was achieved, the cue was covered, and a second blue square was presented indicating the location of the required second saccade. The position of this blue square indicated to the subject the type of trial being experienced. If the blue square was for the second cue of the same option, the subjects were in an option trial, whereas if the blue square was for the same attribute cue of the second option, then the subjects were in an attribute trial. The selection of trial types was pseudorandom. After the subject made a saccade to the blue square, the blue square was replaced by the picture cue, and the subject was again required to maintain fixation on the second cue for 300 ms. After that point, the subjects were relatively unconstrained. The two remaining unexplored locations were then replaced by blue squares. The subject could either choose an option via joystick movement (left/right) on the basis of the value of the currently known information or saccade to one or both of the remaining cues (in any order) as they wanted (with the third cue requiring 300 ms of fixation before the subjects could saccade and uncover the information of the fourth cue) before making a choice. Importantly, however, they were prevented from viewing any cue that they had already seen. After a response was made, all four cues were uncovered (for 500 ms for subject F and 1,000 ms for subject M), after which juice-reward feedback was given with the probability and reward magnitude chosen by the subject.

Notably, the positions of the probability/magnitude cues were counterbalanced across trials; i.e., in half of all option/attribute trials, the probability cues appeared in the top row, and in the other half of trials, the magnitude cues appeared in the top row. Attribute locations also corresponded across options (i.e., if the probability was in the top row for the left option, it would also be in the top row for the right option). Additionally, the location of the first cue was counterbalanced across all four possible spatial locations across trials.

Option and attribute trials were pseudorandomly interleaved during blocks of 50 trials. Between each of these blocks, subjects were presented with a block of 25 trials, in which all four picture cues were presented immediately (so-called 'simultaneous' trials). Data from these trials will be discussed in a separate publication.

Neuronal recordings. Subjects were implanted with a titanium head positioner for restraint, then subsequently implanted with two recording chambers that were located on the basis of preoperative 3 T MRI and stereotactic measurements. Postoperatively, we used gadolinium-attenuated MRI imaging and electrophysiological mapping of gyri and sulci to confirm chamber placement. The center of each chamber along the anterior–posterior (AP) coordinate plane was as follows. Subject M: left, AP 30.5; right, AP 33. Subject F: left, AP 34; right, AP 32.5. The chambers were angled along the medial–lateral plane to target different frontal regions (Fig. 3). Craniotomies were then performed inside each chamber to allow for neuronal recordings.

During each recording session, neuronal activity was measured with tungsten microelectrodes (FHC Instruments) that were lowered into the brain through a grid with custom-built manual microdrives or chamber-mounted motorized microdrives (FlexMT; AlphaOmega). During a typical recording session, 8–24 electrodes were lowered bilaterally into multiple target regions until well-isolated neurons were found. Neuronal data was recorded at 40 kHz with a Plexon Omniplex system. Single-unit isolation was achieved with manual spike sorting with a Plexon Offline Sorter. We randomly sampled neurons; no attempt was made to select neurons on the basis of responsiveness. This procedure ensured an unbiased estimate of neuronal activity, thereby allowing for a fair comparison of neuronal properties among the different brain regions. Notably, the neural populations used to perform analyses in Figs. 4–6 were therefore not all simultaneously recorded but instead were pseudopopulations constructed across multiple recording sessions. Each neuron was first averaged across conditions (Fig. 4) or regressed across trials (Figs. 5 and 6) to identify the neuron's response to experimental variables, thus allowing us to collapse data across sessions, as in previous studies with similar approaches[10,39,41]. We excluded neurons with an average firing rate of <1 Hz from further analysis (9 units in the ACC, 21 units in the DLPFC, and 12 units in the OFC; *n* values reported in main text are after these units had been removed). No statistical methods were used to predetermine sample sizes, but our sample sizes were similar to those reported in previous publications (refs [10,11,14,15,20,38–40,42,46]).

We recorded neuronal data from three target regions: the ACC, DLPFC and OFC. We considered the ACC to be the entire dorsal bank of the anterior cingulate sulcus from AP 27–37 mm. Our LPFC recordings spanned both dorsal and ventral banks of the principal sulcus but were concentrated toward the former. All neurons recorded lateral to the medial orbital sulcus and medial to the lateral orbital sulcus were considered OFC. In some sessions, all three regions were recorded simultaneously, whereas in other sessions, only two were targeted. The total number of units with firing rate >1 Hz in each brain region for each recording session is shown in Supplementary Table 1. Some recordings were also made in the ventromedial prefrontal cortex, but those will be discussed in a separate publication. We used the gadolinium-enhanced MRI along with electrophysiological observations during the process of lowering each electrode to estimate the location of each recorded neuron and produce a histological map of the neuronal population (Fig. 3). All data were subsequently analyzed with custom-written MATLAB code, with MATLAB 2017a (MathWorks). Data collection and analysis were not performed blind to the conditions of the experiments, because the neuroanatomical locations of recording sites needed to be known during lowering of electrodes for recording.

Representational similarity analysis at cue 1 presentation (Fig. 4, Supplementary Figs. 2 and 4, and Supplementary Video 1). To calculate the representational similarity matrices shown in Fig. 4a–c, we first calculated the average firing rate for each neuron for each of the 20 conditions of interest: when the lowest-to-highest-probability cues were presented on the left at cue 1, when the lowest-to-highest-magnitude cue was presented on the left at cue 1, when the lowest-to-highest probability cue was on the right, and when the lowest-to-highest-magnitude cue was on the right. This firing rate was computed between 100 ms and 500 ms after the cue 1 onset. We then normalized across these 20 conditions, subtracting the mean and dividing by the s.d.

Repeating this procedure for every neuron yielded a matrix with dimensions (neurons × 20). For two conditions (*i*,*j*), we computed the correlation coefficient across neurons between row *i* and row *j* of this matrix, which is plotted in element (*i*,*j*) of the representational similarity matrix. For Supplementary Video 1, we repeated the same procedure on sliding windows of ±100 ms from the time point of interest.

RSA template-based regression (Fig. 4d–h). We used multiple linear regression to assess the contributions of several potential 'template' neural codes to the RSA matrices within each region. Each of the 400 elements of each region's RSA template was explained with the following regression model:

$$\boldsymbol{r}_{(i,j)} = \beta_0 + \sum_{n=1}^{6} \beta_n \text{template}_{n(i,j)} + \epsilon_{(i,j)}$$

Where $\boldsymbol{r}$ denotes the correlation-coefficient matrix computed with RSA, and there are six template matrices onto which the RSA matrix is regressed. We estimated β_{0-6} with ordinary least squares, minimizing the sum of squared residuals, ε. The six template matrices were as follows:

- Template 1: identity matrix, accounting for all RSA matrices being 1 when element i = element j (this is a regressor of no interest, to model out the unity correlation between a condition and itself)
- Template 2 (Fig. 4d): spatial attention, accounting for representational similarity between cues presented on the same side but dissimilarity between cues on opposite sides (1 if $i \leq 10$ and $j \leq 10$, 1 if $i \geq 11$ and $j \geq 11$, −1 elsewhere)
- Template 3 (Fig. 4e): stimulus identity, accounting for representational similarity between the same stimulus being presented in left/right options (1 where $|i - j| = 10$, 0 elsewhere)
- Template 4 (Fig. 4f): attended value, accounting for representational similarity between similarly valued items and representational dissimilarity between dissimilarly valued items (ranked value(i) × ranked value(j), where ranked value is −2 for the lowest-ranked stimulus within an attribute (i.e., 10% probability, 15%-maximal reward magnitude), −1 for the second-lowest-ranked (30% probability, 35%-maximal reward magnitude), 0 for the median ranked (50% probability, 55%-maximal reward magnitude), 1 for the second-highest-ranked (70% probability, 75%-maximal reward magnitude) and 2 for the highest-ranked (90% probability, 95%-maximal reward magnitude)). Further justification of the structure of this regressor is provided in the Supplementary Note.
- Template 5 (Fig. 4g): left/right value, interaction of template 4 with spatial attention, i.e., set to the same value as template 4 for cues presented on the same side, and set to 0 for cues presented on opposite sides
- Template 6 (Fig. 4h): accept/reject, accounting for representational similarity between cues that might lead to ultimate acceptance of the current alternative (good items similar to other good items; bad items similar to other bad items), and representational dissimilarity between dissimilar items in terms of acceptance/rejection ('sign of attended value' template)

For the middle panels in Fig. 4d–h, this model was estimated for RSA matrices from 100–500 ms poststimulus, as in Fig. 4a–c; for the bottom panels of Fig. 4d–h, it was performed on sliding windows of ±100 ms from the time point of interest, as in Supplementary Video 1. In these panels, we plotted the CPD for each regressor over time, which is defined for explanatory variable (EV) X_i as follows:

$$\mathrm{CPD}(X_i) = [\mathrm{SSE}(X_{\sim i}) - \mathrm{SSE}(X_{\sim i}, X_i)] / \mathrm{SSE}(X_{\sim i})$$

where SSE(X) refers to the sum of squared errors in a general linear model (GLM) that includes a set of EVs X, and $X_{\sim i}$ is a set of all the EVs included in the full model except X_i (refs [14,40]).

Before running the regression model, we normalized each template by dividing by its maximum absolute value (so that the minimum possible value of each template was −1, and the maximum value of each template was + 1). This normalization was simply to place the regressors on a common scale, so that when plotted the results in Fig. 4, the same color axis could be used to describe all regressors. Importantly, this normalization has no bearing on either the CPD or t statistics, because both of these measures are scale free.

To quantify the latency at which different factors were represented over time, we calculated the time point at which the CPD reached 75% of its maximal value over time, a statistic we term t_{75} in the paper. To simulate how different instantiations of the noise might have affected our estimate of t_{75}, we permuted the residuals from the original GLM and added these permuted residuals to $X\beta$ (where X is the design matrix, and β are the parameter estimates). We then recalculated the time-varying measure of CPD and reestimated t_{75} for each instantiation of the noise. The resulting distribution of values of t_{75} from this analysis are shown in Supplementary Fig. 5c (100 permutations were performed).

Statistical inference on RSA template-based regression model. We tested the significance of each template within each region by computing the t statistic for each β coefficient (i.e., $\hat{\beta}_n / \hat{\sigma}_n$, where $\hat{\sigma}_n$ denotes the standard errors of each coefficient estimate). We compared differences between regions by computing F statistics equivalent to a one-way ANOVA (https://fsl.fmrib.ox.ac.uk/fsl/fslwiki/FEAT/UserGuide#ANOVA:_1-factor_4-levels, for example). Importantly, however, when calculating these statistics on a correlation matrix, they may not be parametrically distributed in the null distribution (owing to observations not being independently and identically distributed). To overcome this, we built a nonparametric null distribution for each test of interest, by permuting the identities of the 20 cues (i.e., values 1–5 on probability/magnitude, left/right), recomputing the RSA matrix and rerunning the regression. We then computed the t statistics and F statistics on this permuted data, and compared the true statistics to the permuted null distribution to obtain P values[54]. We performed 10,000 permutations.

General linear model underlying analyses in Figs. 5–7. For the analyses shown in Figs. 5–7, we first estimated a GLM on the firing rate of each individual neuron, time-locked with respect to cue 1 presentation, cue 2 presentation, cue 3 presentation and joystick movement (response). Each neuron's firing rate was explained with a GLM containing 18 EVs, detailed below, estimated with ordinary least squares. Of note, EVs 1–6 are critical for the analyses shown in Fig. 5 and Supplementary Figs. 6 and 7; EVs 13–16 are critical for the analyses shown in Fig. 6a–c and Supplementary Fig. 10; and EVs 17–18 are critical for the analyses shown in Fig. 6d.

EV 1 captured the linear effect of changing the first attended cue's value from the lowest value to the highest value, collapsing across probability and magnitude cues, selectively in option trials. Specifically, if the lowest-ranked probability/magnitude item was presented, they were valued −2; if the second-lowest-ranked item was presented, they were valued −1; if the third-lowest-ranked item was presented, they were valued 0; if the second-highest-ranked item was presented, they were valued 1; and if the highest-ranked item was presented, they were valued 2.

EVs 2–4 were similar to EV 1 but reflected the values of the second, third and fourth attended cues, respectively (for option trials only). In trials in which the third or fourth cue was not attended to in an option trial (because the subject responded without sampling all cues), the corresponding EVs were valued 0.

EVs 5 and 6 were similar to EVs 1 and 2 but reflected the values of the first and second attended cues, respectively, for attribute trials only. EVs 7 and 8 were similar to EVs 3 and 4 but reflected the values of the third and fourth attended cues in attribute trials in which the subject saccaded diagonally back to the first side of the screen (0 in vertical saccade trials), whereas EVs 9 and 10 reflected the values of the third and fourth attended cues in attribute trials in which the subject saccaded vertically to the second side of the screen (i.e., 0 in diagonal saccade trials). Notably, there was no need to split option trials by the third-saccade direction, because the third saccade was always to the second side of the screen.

EV 11 was an indicator variable for option trials (1 in option trials, 0 otherwise), and EV 12 was an indicator variable for attribute trials (1 in attribute trials, 0 otherwise). Notably, EVs 11 and 12 summed to a constant term, thereby capturing variation in the mean firing rate of the cell across time.

EVs 13–16 were variables that captured the extent to which the cue values observed at cue 2 and cue 3 were consistent (belief confirmation) or inconsistent (belief disconfirmation) with the currently held belief as to which option would be rewarded. They are described below, but for clarity, they are also depicted in Supplementary Fig. 8. Two key points are pertinent: (i) by design, all four EVs were largely orthogonal to the values of cue 1, cue 2 and cue 3 (although see note on EV 16 below); (ii) each of the EVs relied upon different cues and different trials, and so were orthogonal to one another by design.

EV 13 (Supplementary Fig. 8a) was the same as EV 2, i.e. the value of cue 2 in option trials, but crucially, it was multiplied by 1 whenever the value of the first cue was greater than the average value (i.e., best or second-best picture cues), multiplied by −1 whenever the value of the first cue was lower than the average value (i.e., worst or second-worst picture cue), and multiplied by 0 whenever it was of average value (middle picture cue). EV 13 therefore was positively signed whenever cue 2 was consistent with cue 1 (for example, a low-valued cue followed by another low-valued cue, or a high-valued cue followed by another high-valued cue).

EV 14 (Supplementary Fig. 8b) was the same as EV 6, i.e. the value of cue 2 in attribute trials, but was multiplied by 1 when the first cue's value was lower than average, by −1 whenever the first cue's value was higher than average, and by 0 when cue 1 was of average value. Again, this meant that EV 14 was positively signed whenever it was consistent with cue 1 (for example, a low-valued cue on the left followed by a high-valued cue on the right both favored the right action, or a high-valued cue on the left followed by low-valued cue on the right both favored the left action).

EV 15 (Supplementary Fig. 8c) was the same as EV 3, i.e., the value of cue 3 in option trials, but was multiplied by 1 whenever the first and second cue were lower than average value (when EV 1 + EV 2 was negative), by −1 whenever the first and second cue were higher than the average value (when EV 1 + EV 2 was positive), and by 0 when the first and second cue were of average value (when EV 1 + EV 2 equaled 0).

EV 16 (Supplementary Fig. 8d) was defined similarly to EVs 7 and 9, i.e. the value of cue 3 in attribute trials, but crucially relied upon an interaction of the relative value of the first and second cue, and on which side the subject decided to attend with the third saccade. In trials in which the subject's third saccade was diagonal back to option 1, it was EV 7 multiplied by 1 when EV 5 > EV 6; multiplied by −1 when EV 6 > EV 5; and multiplied by 0 when EV 5 = EV 6. In trials in which the subject's third saccade was vertical within option 2, it was EV 9 multiplied by 1 when EV 6 > EV 5; multiplied by −1 when EV 5 > EV 6; and multiplied by 0 when EV 5 = EV 6. Of note, because subjects' decisions whether to make a third saccade to the same side as option 1 relied upon the relative values of cue 1 and cue 2, there was a positive correlation between EV 16 and EVs 7 and 9 (mean r^2 of 0.167 and 0.194, respectively; Supplementary Fig. 9). Nevertheless, including all three EVs together in the GLM directly controlled for this correlation with value, by partialing out any variance attributable to EVs 7 or 9 from the parameter estimate for EV 16.

EV 17 was defined in terms of action selectivity in option trials. It was valued 1 in option trials in which the subject chose left, −1 in option trials in which the subject chose right and 0 in attribute trials.

EV 18 was defined in terms of action selectivity in attribute trials. It was valued 1 in attribute trials in which the subject chose left, and −1 in attribute trials in which the subject chose right.

We estimated this multiple-regression model of the neuronal firing rate in sliding 200-ms bins, stepped in 10-ms time windows, from 100 ms precue to 500 ms postcue (when stimulus locked), or from 500 ms preresponse to 100 ms postresponse (when response locked). We excluded trials in which the subjects viewed fewer than three cues from this analysis.

Peristimulus correlation and cross-correlation of parameter estimates from GLM (Fig. 5 and Supplementary Figs. 6 and 7). After the model in the previous section was estimated for each neuron, we then correlated, across neurons, the *t* statistics associated with parameter estimates for different EVs. This procedure allowed us to examine how population subspaces encoding different variables related to each other, at various time points through the trial. Notably, in one case (Fig. 5b), we collapsed across parameter analyses from option and attribute trials for clarity. Parameter estimates in Fig. 5b–f, k were taken from 250 ms after stimulus, whereas in Fig. 5g–j, they were repeated on all possible combinations of time points to produce cross-correlation matrices of parameter estimates. In Fig. 5k, we performed a Fisher *r*-to-*z* transformation to test the differences between these correlations among subregions.

Statistical inference on cross-correlation of parameter estimates. To test whether areas of high/low correlation between parameter estimates were significantly larger than would be expected by chance, we used a cluster-based permutation test[54]. We identified clusters in the cross-correlation map that were larger than a cluster-forming threshold (set at $|r| > 0.2$; similar results were obtained with other cluster-forming thresholds). We then permuted (across neurons) one of the two sets of parameter estimates used to compute the cross-correlation matrix, and we identified clusters that exceeded the cluster-forming threshold in the permuted data. For each of the 1,000 permutations, we stored the size of the largest cluster. This procedure provided a null distribution of maximum cluster sizes that would be expected by chance. We used percentile 99.9 of this null distribution as a threshold for deeming whether the cluster sizes observed in the data were significant, at $P < 0.001$ (corrected for multiple comparisons).

Projection of ACC activity onto belief confirmation/chosen response subspaces (Fig. 6, Supplementary Fig. 10 and Supplementary Video 2). To identify whether there was a stable subspace representing belief confirmation in each brain region (Fig. 6a), we investigated whether the parameter estimates for all four regressors that captured belief confirmation in our GLM were correlated (Supplementary Fig. 9). The parameter estimates used were EV 13, 300 ms after cue 2 onset; EV 14, 300 ms after cue 2 onset; EV 15, 300 ms after cue 3 onset; and EV 16, 300 ms after cue 3 onset. We also asked whether this subspace was similar to the subspace for cue 1 value (i.e., EV1 + EV5, 300 ms after cue 1 onset), on the basis of the idea that cue 1 'value' responses in the ACC are better conceived in terms of belief confirmation about accepting or rejecting the first attended cue (cf. results in Fig. 4c, h). We again performed a Fisher *r*-to-*z* transformation to test the differences across subregions between the correlations in these subspaces.

This approach uniquely identified a stable subspace for belief confirmation in the ACC. After this stable subspace was identified (Fig. 6a and Supplementary Fig. 10), we asked how activity in this subspace evolved in trials in which the subject took different lengths of time to make a final choice response (Fig. 6 and Supplementary Video 2). For each neuron, we split trials into five separate bins depending on the response time from cue 1 onset, then averaged neuronal firing for these different trial types. For each bin, this procedure yielded a matrix with dimensions time × neurons.

To examine activity within different subspaces, we then regressed this matrix onto a projection matrix composed of two key 'weights' per neuron, i.e., *t* statistics of contrasts of parameter estimates of interest, estimated from the GLM. This projection matrix therefore had dimensions neurons × (2 PEs). The two contrasts of interest were: (i) the average parameter estimates for belief confirmation, i.e., EV 13, 300 ms after cue 2 onset; EV 14, 300 ms after cue 2 onset; EV 15, 300 ms after cue 3 onset; and EV 16, 300 ms after cue 3 onset; and (ii) the average parameter estimates for left-versus-right action selection, i.e. EV 17 and EV 18, 200 ms before response onset.

Regressing the time × neurons matrix onto the neurons × (2 PEs) gave rise to the sliding analysis in Fig. 6. In Fig. 6b, c, we plotted the stimulus-locked and response-locked parameter estimates for contrast 1, respectively, reflecting the population activity in the belief-confirmation subspace for trials of different length. In Fig. 6d, we plotted the response-locked parameter estimates for contrast 2, reflecting population activity in the left/right action-selection subspace in trials of different length. In both cases, we baseline corrected subspace activity to the time of cue 1 onset ±50 ms. Supplementary Video 2 provides a representation of how activity in both of these subspaces progressed during the course of the trial.

Crucially, we avoided using the same data for estimating different neurons' weights in the projection matrix and for plotting population activity. To do so, we first split the data into odd and even trials; we estimated the projection-matrix weights with the GLM in the odd trials, and projected those weights onto firing rates in the even trials; we then repeated the same process with even trials for GLM estimation and odd trials for projection; finally, we averaged subspace activity together across odd and even trial analyses.

Reporting Summary. Further information on research design is available in the Nature Research Reporting Summary linked to this article.

Code availability. The custom MATLAB analysis scripts that support the findings in this study have been made freely available for download at the CRCNS data repository (http://crcns.org/) under dataset pfc-7 (ref. [55]).

Data availability

The raw neuronal data that support the findings in this study have been made freely available for download at the CRCNS data repository (http://crcns.org/) under dataset pfc-7 (ref. [55]).

References

51. Asaad, W. F. & Eskandar, E. N. A flexible software tool for temporally-precise behavioral control in Matlab. *J. Neurosci. Methods* **174**, 245–258 (2008).
52. Asaad, W. F. & Eskandar, E. N. Achieving behavioral control with millisecond resolution in a high-level programming environment. *J. Neurosci. Methods* **173**, 235–240 (2008).
53. Asaad, W. F., Santhanam, N., McClellan, S. & Freedman, D. J. High-performance execution of psychophysical tasks with complex visual stimuli in MATLAB. *J. Neurophysiol.* **109**, 249–260 (2013).
54. Nichols, T. E. & Holmes, A. P. Nonparametric permutation tests for functional neuroimaging: a primer with examples. *Hum. Brain Mapp.* **15**, 1–25 (2002).
55. Hunt, L. T., Malalasekera, W. M. N. & Kennerley, S. W. Recordings from three subregions of macaque prefrontal cortex during an information search and choice task. *CRCNS.org,* https://doi.org/10.6080/K0PZ5712 (2018).

Corresponding author(s): Laurence Hunt, laurence.hunt@psych.ox.ac.uk
Steve Kennerley, s.kennerley@ucl.ac.uk

Reporting Summary

Nature Research wishes to improve the reproducibility of the work that we publish. This form provides structure for consistency and transparency in reporting. For further information on Nature Research policies, see Authors & Referees and the Editorial Policy Checklist.

Statistical parameters

When statistical analyses are reported, confirm that the following items are present in the relevant location (e.g. figure legend, table legend, main text, or Methods section).

n/a	Confirmed	
☐	☒	The exact sample size (*n*) for each experimental group/condition, given as a discrete number and unit of measurement
☐	☒	An indication of whether measurements were taken from distinct samples or whether the same sample was measured repeatedly
☐	☒	The statistical test(s) used AND whether they are one- or two-sided *Only common tests should be described solely by name; describe more complex techniques in the Methods section.*
☐	☒	A description of all covariates tested
☐	☒	A description of any assumptions or corrections, such as tests of normality and adjustment for multiple comparisons
☐	☒	A full description of the statistics including central tendency (e.g. means) or other basic estimates (e.g. regression coefficient) AND variation (e.g. standard deviation) or associated estimates of uncertainty (e.g. confidence intervals)
☐	☒	For null hypothesis testing, the test statistic (e.g. *F*, *t*, *r*) with confidence intervals, effect sizes, degrees of freedom and *P* value noted *Give P values as exact values whenever suitable.*
☒	☐	For Bayesian analysis, information on the choice of priors and Markov chain Monte Carlo settings
☒	☐	For hierarchical and complex designs, identification of the appropriate level for tests and full reporting of outcomes
☐	☒	Estimates of effect sizes (e.g. Cohen's *d*, Pearson's *r*), indicating how they were calculated
☐	☒	Clearly defined error bars *State explicitly what error bars represent (e.g. SD, SE, CI)*

Our web collection on statistics for biologists may be useful.

Software and code

Policy information about availability of computer code

Data collection	The behavioral paradigm was run using the MATLAB based toolbox MonkeyLogic (http://www.monkeylogic.net/, Brown University, USA). Neuronal data was recorded at 40kHz using a Plexon Omniplex system (Dallas, USA)
Data analysis	Single unit isolation was achieved with manual spike sorting, using Plexon Offline Sorter (Dallas, USA). All data was subsequently analysed using custom-written MATLAB code, using MATLAB 2017a (MathWorks, Natick, USA).

For manuscripts utilizing custom algorithms or software that are central to the research but not yet described in published literature, software must be made available to editors/reviewers upon request. We strongly encourage code deposition in a community repository (e.g. GitHub). See the Nature Research guidelines for submitting code & software for further information.

Data

Policy information about availability of data

All manuscripts must include a data availability statement. This statement should provide the following information, where applicable:

- Accession codes, unique identifiers, or web links for publicly available datasets
- A list of figures that have associated raw data
- A description of any restrictions on data availability

The raw neuronal data and custom MATLAB analysis scripts that support the findings in this study will be made freely available for download on the CRCNS data repository (http://crcns.org) upon publication.

Field-specific reporting

Please select the best fit for your research. If you are not sure, read the appropriate sections before making your selection.

☒ Life sciences ☐ Behavioural & social sciences ☐ Ecological, evolutionary & environmental sciences

For a reference copy of the document with all sections, see nature.com/authors/policies/ReportingSummary-flat.pdf

Life sciences study design

All studies must disclose on these points even when the disclosure is negative.

Sample size	Sample size for macaque recording studies is normally constrained to be n=2 macaques for ethical reasons, and is standard across virtually all macaque electrophysiology studies. Sample size for appropriate number of neurons was determined based on past studies (e.g. Kennerley et al., Nat Neuro 2011; Kennerley et al., J. Neurosci 2009)
Data exclusions	Neurons with an average firing rate of <1Hz were excluded from further analysis, as is common in electrophysiology studies, as the low firing rate of these cells means that they are not well-suited to analysis via linear regression etc. In the main general linear model used in Figures 5-7, regressors were only defined for trials in which the subject sampled 3 or more cues, hence trials where subjects sampled fewer than 3 cues were excluded from this analysis. Both of these exclusion criteria were determined prior to conducting these analyses.
Replication	Key experimental findings were found to replicate across both macaques studied (see e.g. main Fig. 1, Fig. S1, S2)
Randomization	Not relevant (animals were not studied in groups). Neurons were grouped into different brain regions; neurons were randomly sampled from these different brain regions without pre-screening for functional selectivity etc.
Blinding	Investigators were not blinded to brain region, as neuroanatomical location of recording sites had to be known when lowering electrodes for recording.

Reporting for specific materials, systems and methods

Materials & experimental systems

n/a	Involved in the study
☒	☐ Unique biological materials
☒	☐ Antibodies
☒	☐ Eukaryotic cell lines
☒	☐ Palaeontology
☐	☒ Animals and other organisms
☒	☐ Human research participants

Methods

n/a	Involved in the study
☒	☐ ChIP-seq
☒	☐ Flow cytometry
☒	☐ MRI-based neuroimaging

Animals and other organisms

Policy information about studies involving animals; ARRIVE guidelines recommended for reporting animal research

Laboratory animals	Two adult male rhesus monkeys (Macaca mulatta; approx 4 years old at start of experiment) were used as subjects and weighed 7-10kg at the time of neuronal data collection.

Wild animals	This study did not involve wild animals.
Field-collected samples	This study did not involve field-collected samples.